Radiometry for **O**cean Colour **SA**tellites **C**alibration & Community **E**ngagement

ESTIMATED UNCERTAINTY BUDGET (EUB)

This page is intentionally left blank

Project deliverables

Id	Content	Document (file name)
PDD	Preliminary design document	ROSACE_PDD_LOV_ v4.0 _20191121.doc
PPD	Preliminary planning document	ROSACE_PPD_ ACRI_v4.0 _20191121.doc
PCD	Preliminary costing document	ROSACE_PCD_ ACRI_v4.0 _20191121.doc
EUB	Estimated uncertainty budget	ROSACE_EUB_ NPL_v4.0 _20191121.doc

Signature

	Name	Company or Institute	Signature
Prepared by	Agnieszka Białek Sam Hunt Bertrand Saulquin Véronique Bruniquel	National Physical Laboratory, UK Acri-ST	
Reviewed by			
Authorized by			

Table of Content

List of Tables

List of Figures

1 INTRODUCTION

1.1 Scope of the Document

This document is the Estimated Uncertainty Budget for the Copernicus Ocean Colour Vicarious Calibration (OC-SVC) Infrastructure. It is one of the deliverables of the ROSACE project funded by EUMETSAT ref. EUMCO184600002162EJK.

This document was supposed to accompany the excel EUB.xlsx version where information is presented in tabular form only, however it become the main deliverable, as the method described here was highly unadaptable to the excel spreadsheet form.

1.2 Structure of the document

The general overview of uncertainty analysis is briefly presented in the chapter 2. The next chapter describes the processing chain for all the elements used in SVC process the main quantities of interest which are water leaving radiance and downwelling irradiance measured *in situ*, normalised water leaving radiance and water-leaving reflectance as the input to the SVC processor, individual match up gains and the mission averaged gain. Chapter 4 contains the details discussion of all uncertainty contributors. Then the uncertainty propagation method is outlined. Chapter 6 contains the results and is followed by the Conclusions.

1.3 APPLICABLE DOCUMENTS

Id	Description	Reference
AD-1	Requirements for Copernicus Ocean Colour Vicarious Calibration Infrastructure (Mazeran, Brockmann, Ruddick, Voss, & Zagolski, 2017b)	EUM/CO/16/4600001772/EJK Available from: https://www.eumetsat.int/website/home/Data/ScienceActivities/index.html
AD-2	SoW for "Preliminary Design of the Copernicus Ocean Colour Vicarious Calibration: Infrastructure, Project Planning and Costing	EUM/RSP/SOW/17/938193 V1F, 4 March 2018
AD-3	OLCI Vicarious Calibration for the VISible bands, Arci- ST Technical Note	Ref. : OLCI.ACR.TN.001, Version : 1.0 Date : 08/09/2019

1.4 Acronyms

The list of the acronyms used in this document is provided hereafter:

Acronym	Definition
AVHRR	Advanced Very High Resolution Radiometer
BPAC	Bright Pixel Atmospheric Correction
BOUSSOLE	Bouée pour l'acquisition de Séries Optiques á Long termE
FIDUCEO	Fidelity and uncertainty in climate data records from Earth observations
FCDR	Fundamental climate data records
GUM	Guide to the expression of uncertainty in measurement
IOP	Inherent Optical Properties
LUT	Look up table
MCM	Monte Carlo Method
MERIS	MEdium Resolution Imaging Spectrometer
MERMAID	MEris MAtchup In-situ Database
MOBY	Marine Optical Buoy
NIR	Near InfraRed
NMI	National Measurement Institute
OC-SVC	Ocean Colour System Vicarious Calibration
OCLI	Ocean and Land Colour Instrument
OCR	Ocean colour radiometry
PDF	Probability Distribution Function
RTM	Radiative Transfer Model
SMART-CC	Stability Monitoring and Absolute RadiomeTric Calibration and Characterisation facility
STAR-OCGE-CC	Spectroscopically Tuneable Absolute Radiometric calibration & characterisation on Ground Support Equipment
TOA	Top of atmosphere
VIS	Visible

2 OVERVIEW OF APPROACH

2.1 Principles of Uncertainty Analysis

The Guide to the expression of Uncertainty in Measurement (GUM), (JCGM100:2008, 2008) provides a framework for how to determine and express the uncertainty of the measured value of a given measurand (the quantity which is being measured). The International Vocabulary of Metrology (VIM), (JCGM200:2012, 2012) defines measurement uncertainty as:

"a non-negative parameter characterizing the dispersion of the quantity values being attributed to a measurand, based on the information used."

The standard uncertainty is the measurement uncertainty expressed as a standard deviation. Please note this is a separate concept to measurement error, which is also defined in the VIM as:

"the measured quantity value minus a reference quantity value."

Generally, the "reference quantity" is considered to be the "true value" of the measurand and is therefore unknown. Figure 2-1 illustrates these concepts.

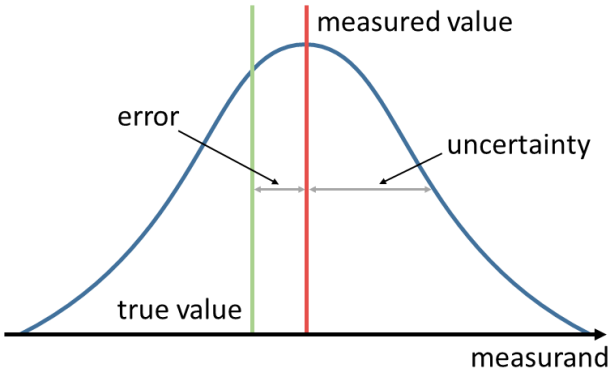

Figure 2-1 – Diagram illustrating the different concepts of measured value and true value, uncertainty and error

Within the GUM framework uncertainty analysis begins with understanding the measurement function. The measurement function establishes the mathematical relationship between all known input quantities (e.g. instrument counts) and the measurand itself (e.g. radiance). Generally, this may be written as,

$$y = f(x_i, \dots, x_N)\,, \qquad \textit{Eq. 1}$$

where:

- y is the measurand;
- x_i are the N input quantities.

Uncertainty analysis is then performed by considering in turn each of these different input quantities to the measurement function, this process is represented in Figure 2-2.

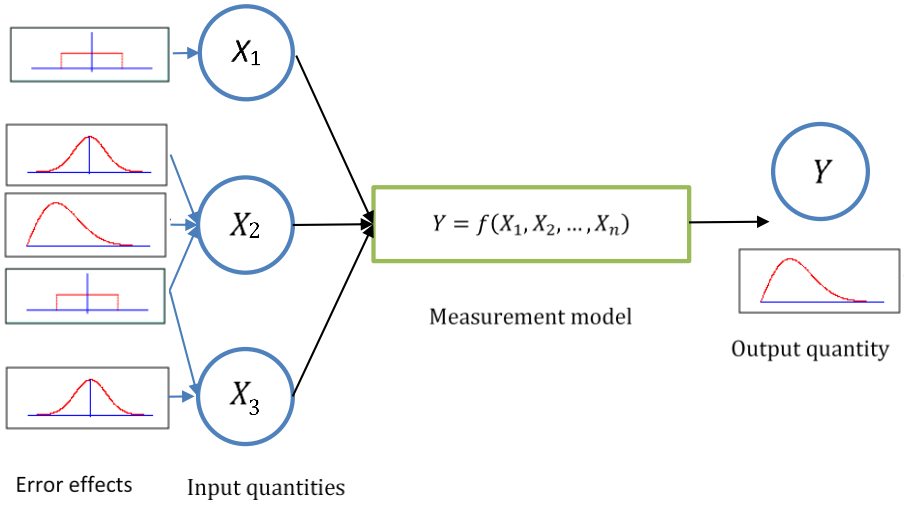

Figure 2-2 – Conceptual process of uncertainty propagation

Each input quantity may be influenced by one or more error effects which are described by an uncertainty distribution. These separate distributions may then be combined to determine the uncertainty of the measurand, $u(y)$, using the *Law of Propagation of Uncertainties* (JCGM100:2008, 2008),

$$u^2(y) = \sum_{i=1}^{N} c_i^2 u^2(x_i) + 2\sum_{i=1}^{N-1}\sum_{j=i}^{N} c_i c_j u(x_i, x_j)\,, \qquad \textit{Eq. 2}$$

where:

- $u^2(y)$ is the combined variance
- $u(y)$ is the combined standard uncertainty, which is the positive square root of the combined variance
- c_i are the sensitivity coefficients of the measurand to the input quantities, $\frac{\partial f}{\partial x_i}$
- $u(x_i)$ are the uncertainties of the input quantities
- $u(x_i, x_j)$ are the covariance between input quantities.

The covariance between input quantities may be written as,

$$u(x_i, x_j) = r(x_i, x_j)u(x_i)u(x_j)\,, \qquad \textit{Eq. 3}$$

where:

- $r(x_i, x_j)$ is the error-correlation coefficient between x_i and x_j (note: $r(x_i, x_j) = r(x_j, x_i)$)

In matrix form the *Law of Propagation of Uncertainties* may be written more conveniently as,

$$u^2(y) = \boldsymbol{c}\boldsymbol{S}(\boldsymbol{x})\boldsymbol{c}^{\mathrm{T}} \qquad \textit{Eq. 4}$$

where:

- $\boldsymbol{c}$ is the vector of sensitivity coefficients, $\left(\frac{\partial f}{\partial x_1} \quad \cdots \quad \frac{\partial f}{\partial x_N}\right)$
- $\boldsymbol{S}(\boldsymbol{x})$ is the error covariance matrix for the input quantities, i.e.,

$$\boldsymbol{S}(\boldsymbol{x}) = \begin{bmatrix} u^2(x_1) & u(x_1, x_2) & \cdots \\ u(x_2, x_1) & u^2(x_2) & \cdots \\ \vdots & \vdots & \ddots \end{bmatrix}$$

In a series of measurements (for a set of match-ups between an in-situ and satellite sensors) it is vital to consider how the errors between the measurements in the series are correlated. This is crucial when evaluating the uncertainty of a result derived from these data.

2.2 FIDUCEO Project Legacy

Within the Horizon 2020 FIDUCEO[1] (Fidelity and uncertainty in climate data records from Earth observations) project a framework was developed to apply rigorous GUM-based metrological methods to satellite sensor fundamental climate data records (FCDRs) to provide per pixel uncertainties. In this document this approach adapted to apply to the Ocean Colour System Vicarious Calibration (OC-SVC). The fundamentals of this approach are described in this section, however please see (Mittaz, Merchant, & Woolliams, 2019) for further details.

2.2.1 Measurement Function Based Analysis

As described in Section 2.1, the basis of the any metrologically rigorous measurement is first understanding how the measurand (e.g. radiance) is determined from a set of input quantities (e.g. detector counts) through a measurement function. Within the FIDUCEO project a schematic representation of the sensor measurement function, called the *uncertainty tree diagram*, formed the basis of the analysis made. Figure 2-3 provides a simplified form of the uncertainty tree diagram for the AVHRR (Advanced Very High

[1] See: https://www.fiduceo.eu

Resolution Radiometer) instrument, a sensor analysed by the FIDUCEO project see (Mittaz, Taylor, Desmons, & Woolliams, 2017).

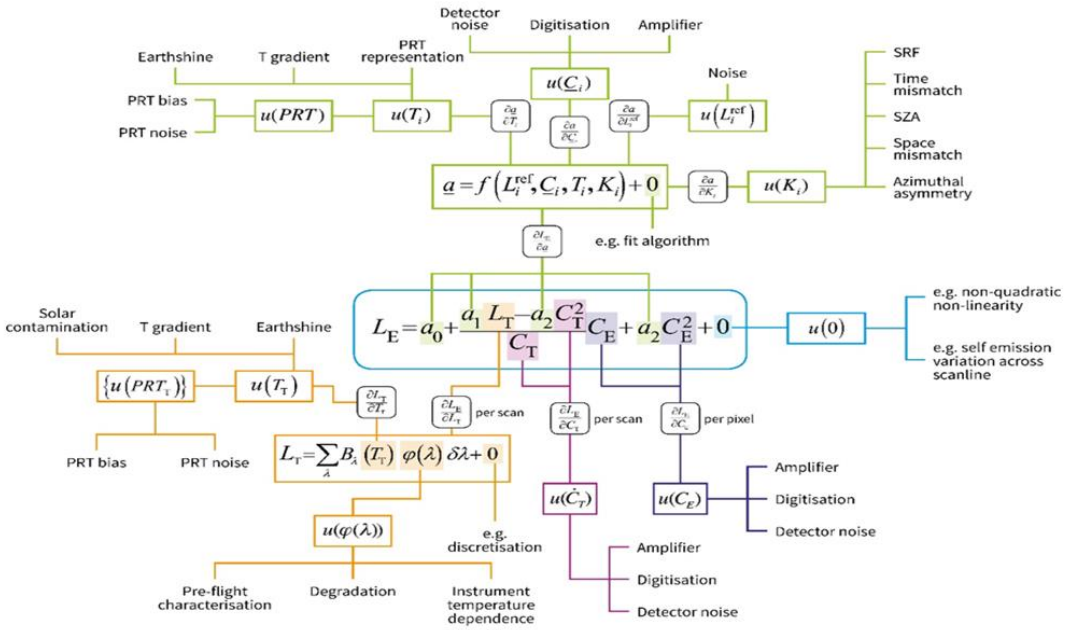

Figure 2-3 – An example Earth Observation sensor uncertainty tree diagram for the AVHRR

At the centre of this diagram is the measurement function for the sensor – here with measurand Earth radiance, L_{E}, and input quantities such as Earth counts, C_{E}, and internal calibration target radiance, L_{T}. From this function branches spread from each input quantity, which may themselves be determined by their own measurement functions (for example here L_{T} is determined from the measured temperature T_{T} of the calibration target), to their uncertainty. This uncertainty can be traced back through to its impact on the measurand by the sensitivity coefficients on each branch. Finally, the effects which cause each respective uncertainty are connected to the end of each branch.

Note that we should also consider the extent to which the measurement function describes the true physical state of the instrument – this is accounted for this by including the term $+0$ at the end of the measurement function. This explicitly represents effects, expected to have zero mean, that are not captured by the measurement function (i.e. there is an uncertainty associated with this quantity being zero).

2.2.2 Effects Tables Reporting

Each of the effects identified at the end of each of the branches should then be understood, quantified and reported in an "Effects Table" which documents:

- The uncertainty associated with the given effect.
- The sensitivity coefficient required to propagate uncertainties associate with that effect to uncertainty associated with the measurand,
- The correlation structure over spatial temporal and spectral dimensions for errors from this effect. The set of FIDUCEO definitions for how this should be reported is contained in Appendix A.

Table 2-1 shows an adapted form of the FIDUCEO "Effects Table" for use in describing error effects in the OC-SVC process, with description of how it should be populated.

Table 2-1- Table for codifying the uncertainty due to an error effect and its correlation structure

Table descriptor		How this is codified
Name of effect		A unique name for each source of uncertainty in a term of the measurement function
Affected term in measurement function		Name and standard symbol of affected term
Instruments in the series affected		Identifier of the specific instrument / deployment where this effect matters
Correlation type and form	Temporal within deployment	Forms of correlation described in Appendix A and detailed fully in(Woolliams, Mittaz, Merchant, & Harris, 2018).
	Temporal between deployments	
	Spectral (hyperspectral in-situ)	
Correlation scale	Temporal within deployment	In units of spectral pixels, measurements or deployments in time – what is the scale of the correlation shape?
	Temporal between deployments	
	Spectral (hyperspectral in-situ)	
Channels/bands	List of channels / bands affected	OLCI channel names in standard form
	Error correlation coefficient matrix	OLCI cross-channel correlation matrix
Uncertainty	PDF shape	Functional form of estimated error distribution for the term
	units	Units in which PDF shape is expressed (units of term, or can be as percentage etc)
	magnitude	Value(s) or parameterisation estimating width of PDF
Sensitivity coefficient		Value, equation or parameterisation of sensitivity of measurand to term

3 OCEAN COLOUR SYSTEM VICARIOUS GAIN MEASUREMENT

The SVC process adjusts the spectral calibration coefficients of the satellite sensors through minimising differences between the observed top of atmosphere (TOA) total radiances and equivalent modelled values. These modelled values are built from *in situ* measurements performed in the best possible conditions combined with atmospheric radiances modelled consistently with the satellite processing algorithms. This adjustment is not only needed because of possibly imperfect calibration of the sensor but also because of unavoidable errors in the atmospheric correction process, by which the dominant part of the signal is quantified to eventually get to the water-leaving radiance L_{w}. This is the quantity of interest and is generally less than 10 % of the total radiance measured by the sensor at the TOA, and often around 5 % only. It was demonstrated that, in such circumstances, achieving a 5 % uncertainty on L_{w} in the blue part of the spectrum, which is a requirement set up rather early in the era of satellite ocean colour radiometry OCR (Gordon & Clark, 1981) was impossible without introducing what is now called a system vicarious calibration (SVC) (Gordon, 1997, 1998).

To sustain SVC for ocean colour sensors (OC-SVC in the following), the solution of deploying permanent moorings in clear open ocean waters has been adopted in the last two decades. The two currently active sites are the Marine Optical Buoy (MOBY; (Clark et al., 1997)) and the Bouée pour l'acquisition de Séries Optiques á Long termE (BOUSSOLE;(Antoine et al., 2006) and PPD document).

The measurements on the buoy are taken in water at fixed depths and the processing chain to derive water leaving radiance from these measurements is described in the following section.

3.1 Processing Steps for *In Situ* Data

3.1.1 One-minute signal acquisitions

The dark corrected signal, S, per instrument is determined as,

$$S = DN_{\mathrm{Light}} - DN_{\mathrm{Dark}}\,, \qquad \textit{Eq. 5}$$

where DN_{Light} and DN_{Dark} are the median light and dark readings, respectively, taken within a one-minute acquisition period. Note that for hyperspectral instruments the total number of readings will vary depending on the integration time per acquisition. This step is applied for all radiometers on the buoy, two radiance and one irradiance.

3.1.2 Calibration to Upwelling Radiance

The upwelling radiance, L_{u,z_1}, measured in water at given depth is given as,

$$L_{u,z_1} = c_{cal}\, c_{stab} c_{\lambda} c_{T} c_{lin} c_{stray} c_{pol} c_{im} c_{sh} c_{fou} S, \qquad \textit{Eq. 6}$$

where the measured signal, S, is first multiplied by calibration coefficient c_{cal}. To correct for instrument optical characteristics the following corrections are then applied:

- c_{stab}– radiometric stability, the actual value is evaluated during post deployment calibration
- c_{λ} – spectral calibration actual central wavelength of each pixel and its accuracy
- c_{T} – temperature correction
- c_{lin} – detector linearity correction
- c_{stray} – spectral stray light correction
- c_{pol} – polarisation sensitivity correction

To correct for the water environment:

- c_{im} – immersion factor
- c_{sh} – shading correction
- c_{fou} – Bio fouling correction

Any of these correction coefficients may be set to 1 if the correction is not required and then we still use them in the equation as a parameter for propagating the uncertainties associated with these effects.

3.1.3 Attenuation Coefficient

The attenuation coefficient is given as,

$$K_{L_u} = -\frac{\ln\left(\frac{L_{u,z_2}}{L_{u,z_1}}\right)}{z_2 - z_1}, \qquad \textit{Eq. 7}$$

where L_{u,z_2} and L_{u,z_1} are the upwelling radiance measurements acquired at two different depths z_1 and z_2.

3.1.4 Depth

Currently, the depth of each radiometer, z_1 and z_2 is calculated from readings of one pressure sensor, buoy tilt and the geometrical configuration of the buoy structure. First, the depth of two arms in the point of contact with the main buoy structure is calculated

$$z_{\mathrm{a1}} = z_{\mathrm{a2}} - \Delta_{12} c_{\mathrm{db}}, \quad \textit{Eq. 8}$$

$$z_{\mathrm{a2}} = z_{\mathrm{sensor}} - \Delta_{\mathrm{SR}} c_{\mathrm{db}}, \quad \textit{Eq. 9}$$

where z_{a1} is the depth of the upper arm, z_{a2} is the depth of the lower arm, z_{sensor} is the depth measured by the pressure sensor, Δ_{SR} is the distance difference between the depth sensor and the lower arm depth at the buoy axis, Δ_{12} is the distance difference between the upper and the lower arms of the buoy in the buoy axis and c_{db} in the buoy depth correction due to the buoy tilt.

Then the actual depth of the instruments attached at the end of each arm are given by

$$z_1 = z_{\mathrm{a1}} + c_{\mathrm{dr}} \Delta_1, \quad \textit{Eq. 10}$$

$$z_2 = z_{\mathrm{a2}} + c_{\mathrm{dr}} \Delta_2 \quad \textit{Eq. 11}$$

Where z_1 and z_2 are the depths of the radiometers at upper and lower arm respectively, c_{dr} is the depth correction for the radiometer that is mounted in the end of buoy's arm and in addition to the buoy depth correction due to the tilt needs to be corrected for the heading of the arm as the instrument depending on the heading can be lower or higher, finally Δ_1 and Δ_2 are the lengths of the upper and lower arm respectively.

The depth measurements will change with the new optical system as then each radiometer will have built in a depth sensor this will reduce uncertainty in the depth evaluation due to geometrical configuration on the buoy to the pressure sensor accuracy only.

3.1.5 Extrapolation to Upwelling radiance just beneath the surface

Upwelling radiance just beneath the surface is given by,

$$\mathrm{L_u}(0^-) = \mathrm{L_{u,z_1}} exp\left(\mathrm{K_{L_u} z_1}\right) f_{\mathrm{h}} \quad \textit{Eq. 12}$$

Taking into consideration all inputs components of the attenuation coefficient equation Eq. 12 becomes,

$$L_{\mathrm{u}}(0^{-}) = L_{\mathrm{u},z_1} \exp\left(-\frac{ln\left(\frac{L_{u,z_2}}{L_{u,z_1}}\right)}{z_2 - z_1} z_1 \right) f_h \qquad \textit{Eq. 13}$$

where f_h is the Hydrolight-based extrapolation correction (Mobley, 1994), that is necessary to account for the multiple scattering and Raman contribution to the upwelling radiance signal especially for the wavelengths above 600 nm.

3.1.6 Water leaving radiance

Water leaving radiance is given by,

$$\boldsymbol{L_w = \frac{1-\rho}{n^2} L_u(0^{-})}\,, \qquad \textit{Eq. 14}$$

where ρ is the Fresnel reflection coefficient for the water-air interface and n is the refractive index of seawater. The fraction $\frac{1-\rho}{n^2}$ is often called water-air constant and is given the approximate value of 0.543 (Austin, 1974; Mueller et al., 2003) .

3.1.7 Normalised water leaving Radiance

The fully normalised water leaving radiance is defined as (Morel & Gentili, 1996),

$$\boldsymbol{L_{wN} = \frac{L_w}{t_d(\theta_s)cos(\theta_s)} \frac{\Re_0}{\Re(\theta')} \left\{ \frac{f_0(Chl)}{Q_0(Chl)} \left[\frac{f(\theta_s, Chl)}{Q(\theta_s, \theta', \Delta\phi, Chl)} \right]^{-1} \right\}}, \qquad \textit{Eq. 15}$$

where $\mathrm{L_{wN}}$ is the normalised water leaving radiance, $\mathrm{t_d}(\theta_s)$ is the downwelling transmittance, $cos(\theta_s)$ is cosine of the solar zenith angle, $\Re_0$ and $\Re(\theta')$ are factors including all refraction and reflection at the air-sea interference, the term in brackets is used to account for BRDF effects with Q the ratio of upward irradiance to upward radiance f is a factor that relates irradiance reflectance to the inherent optical properties. The subscripts $_0$ state normalised conditions , Chl is the chlorophyll a concentration.

The factor of air-sea interface is given by,

$$\boldsymbol{\Re(\theta') = \frac{(1-\bar{\rho})[1-\rho]}{(1-\bar{r}R)n^2}}, \qquad \textit{Eq. 16}$$

where $\bar{\rho}$ is the air-water Fresnel reflection at the interface for the total downwelling irradiance (Sun and sky), ρ is the internal Fresnel reflectance for the associated directions (equivalent to ρ used in equation Eq. 14), $\bar{r}$ is the water–air Fresnel reflection for the whole diffuse upwelling irradiance, R is the upward and downward irradiance ratio at null depth and n is the refractive index of seawater.

The Q factor has units of steradian and is given by

$$\boldsymbol{Q}(\boldsymbol{\theta}', \boldsymbol{\theta}, \boldsymbol{\Delta\phi}) = \boldsymbol{E}_{\mathrm{u}}/\boldsymbol{L}_{\mathrm{u}}(\boldsymbol{\theta_0}, \boldsymbol{\theta}', \boldsymbol{\phi}), \qquad \textit{Eq. 17}$$

Where E_{u} in upward irradiance just beneath the surface and L_{u} is the upwelling radiance at null depth for the geometrical configuration defined in the curly bracket**.** The Q factor in addition depends on, τ , aerosol optical depth, the waves slopes that are related to the wind speed and inherent optical properties such as the single-scattering albedo of the water and the ratio of water molecular backscattering to the total (molecules plus particles) backscattering coefficient. In simplified version IOP can be replaced by wavelengths and chlorophyll concentration, thus considering all variables affecting $\mathrm{Q}(\theta_s, \theta', \Delta\phi, \tau, \lambda, \mathrm{Chl})$**.**

The f factor is used to relate R value with the inherent optical properites,

$$\mathbf{R} = \boldsymbol{f}\,\frac{\boldsymbol{b}_{\mathbf{b}}}{\boldsymbol{a}}, \qquad \textit{Eq. 18}$$

where b_{b} is the backscattering and a is the absorption coefficient.

The parameters $\Re(\theta')$, Q and f are derived from models and applied operationally to the data in the form of look up table (LUT), to estimate uncertainty of those parameters we must link all variables that affects them.

3.1.8 Downwelling irradiance

Downwelling irradiance is measured above the sea surface the instrument is placed on top on the buoy structure. The irradiance sensor has same operational principle for the raw signal acquisition as the previously described radiance instruments (see Eq. 5).

Dark corrected signal is then converted into irradiance, E, using the irradiance calibration coefficient, c_{cal} :

$$E = c_{\mathrm{cal}}\, c_{\mathrm{stab}} c_{\lambda} c_{\mathrm{T}} c_{\mathrm{lin}} c_{\mathrm{stray}} S, \qquad \textit{Eq. 19}$$

To correct for instrument optical characteristics the following corrections are then applied:

- c_{stab}– radiometric stability, the actual value is evaluated during post deployment calibration
- c_{λ} – spectral calibration actual central wavelength of each pixel and its accuracy
- c_{T} – temperature correction
- c_{lin} – detector linearity correction
- c_{stray} – spectral stray light correction

The instrument signal converted to irradiance units has to be process further to correct for the environmental condition during the measurements:

$$E_d = E c_{\cos} f_{tilt} f_{dir} + (1 - f_{dir})\, E c_{\mathrm{hcos}}, \qquad \textit{Eq. 20}$$

where E_d is the final product of the downwelling irradiance, and additional corrections include:

- $c_{\cos}$ – the directional cosine response correction
- c_{hcos} – the hemispherical (diffuse) cosine response correction
- f_{dir} - the fraction of direct to total solar irradiance.
- f_{tilt} - the tilt correction

The tilt correction is applied to the direct component of the E_d measurement. The fraction of direct to total solar irradiance, f_{dir}, component is determined theoretically for clear-sky conditions through the Gregg and Carder (1990) model. The tilt correction, f_{tilt}, of the direct component uses the ratio of the cosine of the sun zenith angle to the cosine of the actual incident angle on the non-level sensor. This correction requires knowledge of the 2-axis tilt values, the sun zenith angle and the sun azimuth, because a given absolute tilt value does not have the same impact whether the buoy is tilted towards the sun or away from it.

3.1.9 Water leaving reflectance

The final step in *in situ* data processing combines the water leaving radiance, L_w, and the downwelling irradiance, E_d, to remote sensing reflectance R_{rs} as the simple ratio of radiance to irradiance or to water leaving reflectance,ρ_w, which is the same ratio multiply by π

$$\rho_w = \pi \frac{L_w(\theta_s,\theta_v,\Delta\phi)}{E_d(\theta_s)}, \qquad \textit{Eq. 21}$$

The water leaving reflectance in the OLCI level 2 product water product.

Both remote sensing reflectance and water leaving reflectance can be normalised by insertion of normalised water leaving radiance to the equation,

$$\rho_{wN} = \pi \frac{L_w(\theta_s,\theta_v,\Delta\phi)}{E_d(\theta_s)} \frac{\Re_0}{\Re(\theta')} \left\{ \frac{f_0(Chl)}{Q_0(Chl)} \left[\frac{f(\theta_s,Chl)}{Q(\theta_s,\theta',\Delta\phi,Chl)} \right]^{-1} \right\}, \qquad \textit{Eq. 22}$$

3.1.10 Uncertainty Tree diagrams

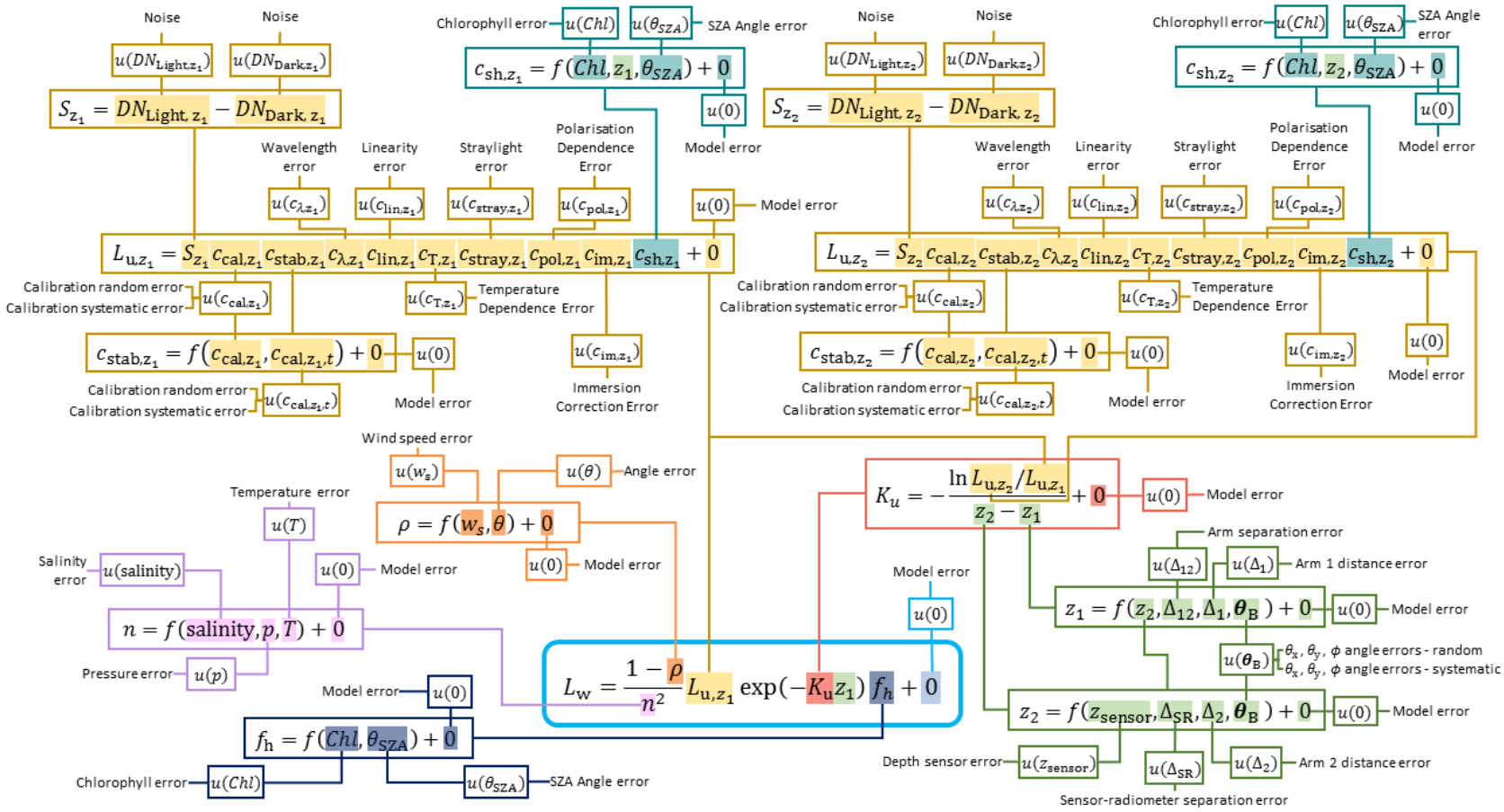

Figure 3-1. Water Leaving Radiance in situ measurement uncertainty tree diagram

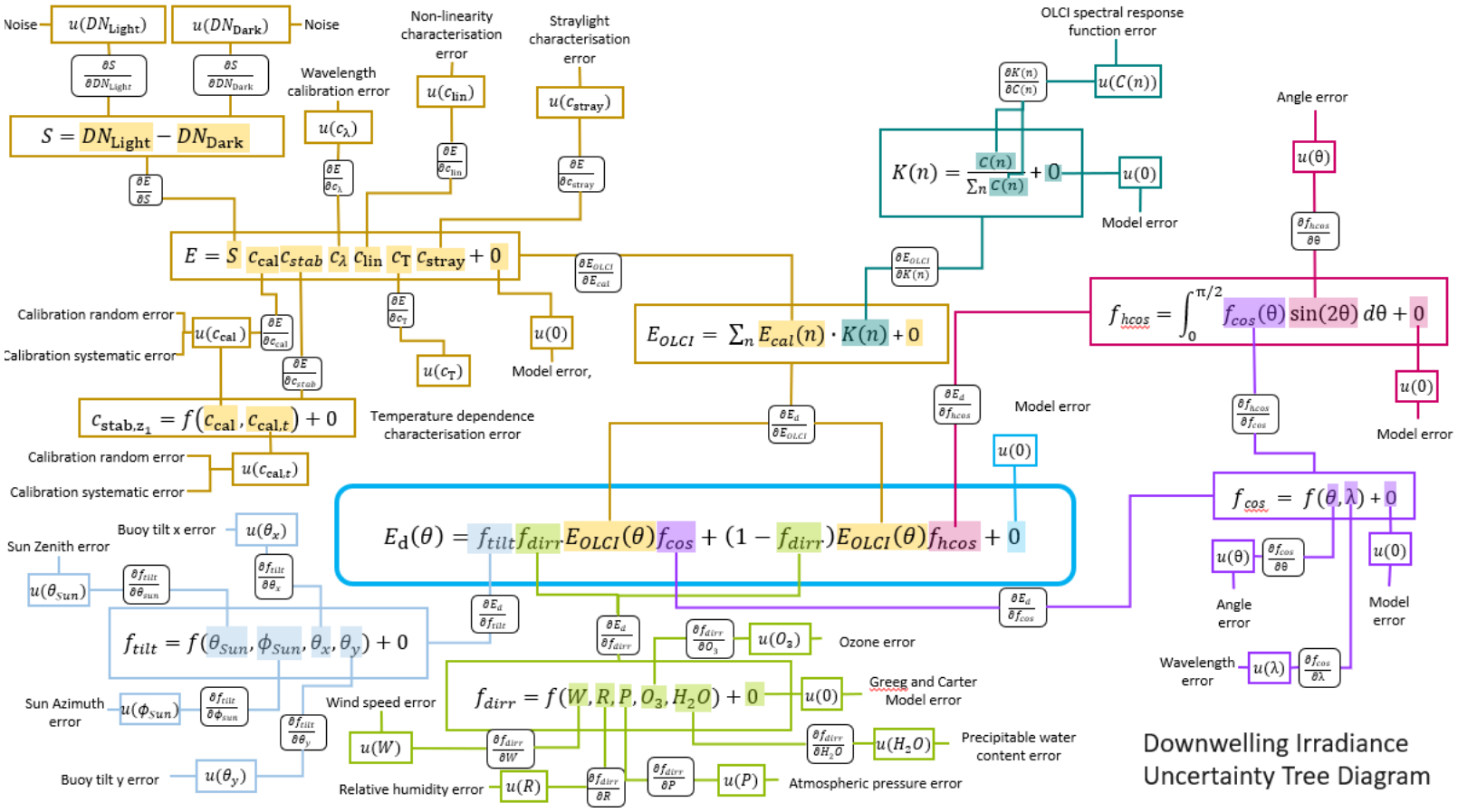

Figure 3-2. Downwelling irradiance in situ measurement uncertainty tree diagram

3.2 Processing Steps for system vicarious calibration gain *(Acri-ST input, AD-3)*

3.2.1 Principle of the vicarious adjustment for OLCI

The primary idea of the vicarious adjustment is to consider that errors in water leaving reflectance come from a systematic bias at TOA, which can be assessed by comparison to reference or *targeted* reflectance ρ_{gc}^{t} on a trustworthy dataset of observations. We note here that ρ_{gc} is equivalent to ρ_{TOA} after some pre-corrections and outside the sun glint (or after correction for it). This problem might come either from an actual bias in the radiometric calibration of the sensor or from inaccuracy of the atmospheric correction based on a radiative transfer modelling. The vicarious adjustment aims at solving blindly the bias issue whatever its exact origin.

For a given target in space and time, hereafter indexed by i, the comparison between the ground truth signal ρ_{gc}^{t} and the measured reflectance ρ_{gc} leads to a local adjustment factor defined by:

$$g(\lambda,i)=\frac{\rho_{gc}^{t}(\lambda,i)}{\rho_{gc}(\lambda,i)}, \qquad \textit{Eq. 23}$$

Provided a statistically representative number of targets, N, and homogeneous individual factors $g(\lambda,i)$, a reliable average gain can then be calculated using a weighted average:

$$G(\lambda)=\frac{\sum_{i=1}^{N} w(\lambda,i)g(\lambda,i)}{\sum_{i=1}^{N} w(\lambda,i)}, \qquad \textit{Eq. 24}$$

where weights are, for instance, the inverse of the uncertainty of each individual gain determined from the sampling standard deviation of OLCI data as well as in situ uncertainty. This means that we give more credence in the least uncertain individual gains.

Once determined, this gain is systematically applied in operation as a multiplicative factor to the measured TOA reflectance $\rho_{gc}(\lambda)$, just before the atmospheric correction step.

It is important to notice that a single set of spectral gains is applied throughout the entire mission and whatever the camera and CCD detector in the field of view. Hence homogeneity in the individual factors $g(\lambda,i)$, should ensure a robust vicarious calibration.

The targeted reflectance, ρ_{gc}^{t},required in the gain computation would ideally be built from concomitant ground measurements of water leaving reflectance, atmospheric aerosol reflectance and atmospheric diffuse transmittance. While reliable *in situ* water leaving reflectances , p_{w}^{IS}, are accessible, simultaneous measurements with aerosol properties are not widely available (Franz, Ainsworth, & Bailey, 2001). To sort out this lack of *in situ* measurements, published procedures have proposed to use the atmospheric variables determined algorithmically by the atmospheric correction above the marine target, after insuring

a proper calibration of the NIR bands (Bailey, Hooker, Antoine, Franz, & Werdell, 2008; Franz, Bailey, Werdell, & McClain, 2007). This means a two-step procedure:

1. First, the NIR bands used in the atmospheric correction, 779 nm and 865 nm, are independently adjusted, if necessary;
2. Then, the atmospheric correction is applied, yielding to path reflectance and transmittance in the VIS bands considered as sufficiently accurate to build the targeted TOA reflectance:

$$\rho_{gc}^{t}(\lambda, i) = \rho_{path}^{vic}(\lambda, i) + t_{d}^{vic}(\lambda, i) \cdot p_{w}^{IS}(\lambda, i), \qquad \text{Eq. 25}$$

where the exponent ^{vic} stands for vicariously adjusted quantities.

An advantage of this approach, pointed out in the first works of NASA, is to decouple the NIR and VIS gains computation and avoid a complex iterative procedure.

Without further atmospheric *in situ* measurement, the first step needs assumptions on the aerosol signal in the NIR. This can be either by fixing an aerosol model already tabulated in the ground segment (*e.g.*(Franz et al., 2007)), or by making an assumption on the spectral shape.

3.2.2 Domain of applicability

The primary unknown in, $\rho_{gc}^{t}(\lambda)$, being the water leaving reflectance and the aerosol reflectance (see Eq. 25), we have decided to put ourselves in situation of stable and homogeneous marine and aerosol properties, *i.e.* avoid coastal areas to weaken the influence of highly variable and complex waters and assemblage of aerosol particles.

3.2.3 Implementation of the vicarious adjustment

3.2.3.1 Overview of the OLCI reprocessing Level 2 chain

We give here an overview of the Level 2 processing chain and detail where the vicarious adjustment has been inserted. Depency on the geometrical angles θs, θv and $\Delta\varphi$ is not made explicit.

OLCI Level 1 products correspond to geolocated and calibrated TOA radiances $L_{TOA}(\lambda)$. The Level 2 chain starts by converting the Level 1 data into TOA reflectances, $\rho_{TOA}(\lambda)$. Then, several processings are sequentially applied, at a pixel level:

- a pixel identification allowing to flag Cloud, Water and Land pixels and guide the next processing steps into the corresponding branches
- a correction of the total gaseous absorption for O_3, O_2, NO_2, and H_2O, leading to TOA reflectance corrected for gaseous absorption, $\rho_{ng}(\lambda)$, related to $\rho_{TOA}(\lambda)$ through:

$$\rho_{TOA}(\lambda) = t_g(\lambda) \cdot \rho_{ng}(\lambda), \quad \textit{Eq. 26}$$

- a glint correction removing the glint reflectance estimated at sea level by the Cox and Munk (1954) model and propagated at TOA by a simplified transmittance $t(\lambda)$ (see (Cox & Munk, 1954), and (MERIS ATBD 2.13, n.d.)) depending only in the Rayleigh optical thickness. This correction leads to the glint-corrected reflectance $\rho_{gc}(\lambda)$ related to $\rho_{ng}(\lambda)$ through:

$$\rho_{ng}(\lambda) = \rho_{gc}(\lambda) + t(\lambda) \cdot \rho_g(\lambda), \quad \textit{Eq. 27}$$

where $t(\lambda)\rho_g(\lambda)$ is the glint reflectance at TOA level.

- the smile, Bodhaine, and pressure adjustment (see (Santer & Zagolski, 2017)for details) reducing the in-field of view variation of channels central wavelengths, correcting for the latitudinal dependency of the Rayleigh optical thickness, and adjusting the signal to P_{std}, the standard pressure of the radiative transfer look-up-tables (LUTs):

$$\rho_{gc}(\lambda) \rightarrow \rho^*_{gc}(\lambda, P_{std}) \quad \textit{Eq. 28}$$

where $\rho^*_{gc}(\lambda)$ is the TOA reflectance corrected for gaseous absorption, glint, smile, Bodhaine latitudinal dependency of Rayleigh optical thickness, and pressure ("all"-corrected)

- the Bright Pixel Atmospheric Correction (BPAC) removing turbid water contributions to the TOA signal as well as NIR calibration residuals in the NIR only:

$$\rho_{path}(\lambda_{NIR}, P_{std}) = \rho^*_{gc}(\lambda_{NIR}, P_{std}) - \mathrm{t}\rho_{wc2}(\lambda_{NIR}, P_{std}), \quad \textit{Eq. 29}$$

Where $\mathrm{t}\rho_{wc2}(\lambda)$ is the TOA water-leaving reflectance retrieved by the Bright Pixel Atmospheric Correction at 709 nm, 779 nm, 865 nm and 885 nm

- the Antoine and Morel atmospheric correction estimating the atmospheric path reflectance and the transmittance related to combined aerosols and Rayleigh effects in the VIS from the NIR

$$\rho_{path}(\lambda_{NIR}, P_{std}) \rightarrow \rho_{path}(\lambda, P_{std}) \text{ and } t_d(\lambda, P_{std}), \quad \textit{Eq. 30}$$

- at this stage these "all"-corrected reflectances can be related to the water pixels by:

$$\rho_{gc}^{*}(\lambda, P_{std}) = \rho_{path}(\lambda, P_{std}) + t_d(\lambda, P_{std}) \cdot \rho_w(\lambda). \quad \textit{Eq. 31}$$

The atmospheric path reflectance, $\rho_{path}(\lambda, P_{std})$, and the total transmittance, $t_d(\lambda, P_{std})$, are given the dependency on P_{std} which is implicit through their computation but is important to mention for the following. Once the spectrum $\rho_w(\lambda)$ is retrieved, the further steps of the Level 2 chain deal with bio-optical inversions.

3.2.3.2 Interpolation scheme for the water-leaving reflectance

In the formulation of $\rho_{gc}^{*}(\lambda, P_{std})$there is no pressure dependency of the water-leaving reflectance, $\rho_w(\lambda)$, because it is not dependent on the atmospheric state. It means that any value P_{std} used for simulating the atmospheric state must, in principle, lead to the same results.

This is not completely true in practice as the pressure (or so-called "Rayleigh") adjustment is more efficient for small deviations (i.e. when applied using the LUT reference pressure closest to the target geophysical pressure). Specific radiative transfer simulations have been run to deal with high altitude (low pressure) water bodies, the series of LUTs representing the atmospheric state now includes the dependency in P_{std} so that $P_{std} \in \{1040, 1013.25, 970, 900, 800, 700\}$ hPa where it used to be only P_{std}=1013.25 hPa.

An analysis has been conducted to assess the sensitivity of $\rho_w(\lambda)$ to a change in P_{std}. It appeared that a better precision on $\rho_w(\lambda)$ is obtained if the atmospheric correction is made on the two closest pressure levels of the LUTs and then interpolated.

Let P_1 and P_2 be the pressure levels (one of the six levels available) bracketing the target pressure P_{pix}, P_1 being the closest to P_{pix1}.

Mathematically we have:

$$\rho_{gc}^{*}(\lambda, P_1) = \rho_{path}(\lambda, P_1) + t_d(\lambda, P_1) \cdot \rho_w(\lambda, P_1), \quad \textit{Eq. 32}$$

and

$$\rho_{gc}^{*}(\lambda, P_2) = \rho_{path}(\lambda, P_2) + t_d(\lambda, P_2) \cdot \rho_w(\lambda, P_2). \quad \textit{Eq. 33}$$

The (Antoine & Morel, 1999) atmospheric scheme is performed only at P_1 to retrieve the aerosol models and mixing ratio (see below for explanations). These are later propagated to $P2$ through interpolation in the LUTs.

Because the pressure adjustment scheme relies on the Rayleigh optical thickness, the interpolation of $\rho_w(\lambda, P_1)$ and $\rho_w(\lambda, P_2)$ is performed using the corresponding Rayleigh optical thicknesses, namely $\tau R(\lambda, P_1), \tau R(\lambda, P_2)$, and $\tau R(\lambda, P_{pix})$.

Defining:

$$\epsilon(\lambda) = \frac{\tau R(\lambda, P_1) - \tau R\left(\lambda, P_{1pix}\right)}{\tau R(\lambda, P_1) - \tau R(\lambda, P_2)}, \qquad \textit{Eq. 34}$$

we have:

$$\rho_w(\lambda) = (1 - \epsilon(\lambda)\,) \cdot \rho_w(\lambda, P_1) + \epsilon(\lambda)\ \cdot \rho_w(\lambda, P_2). \qquad \textit{Eq. 35}$$

3.2.3.3 Methodologies for the vicarious adjustment of the visible bands

To do the vicarious adjustement of the visible bands, one must relate the *in situ* water leaving reflectances $p_w^{IS}(\lambda, i)$ to the "all"-corrected reflectances $\rho_{gc}^*(\lambda, P_1)$and $\rho_{gc}^*(\lambda, P_2)$ or going backwards into the pressure adjustment scheme to relate these to the sole glint-corrected reflectances $\rho_{gc}(\lambda)$ which is less straightforward.

That is now a slight change compared to equation Eq. 23. Two solutions have been proposed, leading to equivalent results, to apply vicarious gains on $\rho_{gc}^*(\lambda, P_1)$ and $\rho_{gc}^*(\lambda, P_2)$:

1. Compute vicarious gains independently for each P_{std} branch, i.e. force the processing to not interpolate between two branches so that only one branch is used for adjustments and atmospheric correction, then compute gains for each of the six branches. In the nominal processing two different sets of vicarious gains would then be applied to $\rho_{gc}^*(\lambda, P_1)$and $\rho_{gc}^*(\lambda, P_2)$respectively.
2. Compute one unique set of vicarious gains to apply on both $\rho_{gc}^*(\lambda, P_1)$ and $\rho_{gc}^*(\lambda, P_2)$.

On an individual basis (i.e. on each matchup between *in situ* measurements and OLCI acquisitions) this leads to solve per wavelength:

$$g(\lambda, i, P_{std}\,) = \frac{\rho_{gc}^{*,IS}(\lambda, i, P_{std})}{\rho_{gc}^*(\lambda, i, P_{std})} = \frac{\rho_{path}(\lambda, i, P_{std}) + \ t_d(\lambda, i, P_{std}\,)\ \cdot \rho_w^{IS}(\lambda, i)}{\rho_{path}(\lambda, i, P_{std}) + \ t_d(\lambda, i, P_{std}\,)\ \cdot \rho_w(\lambda, i)} \qquad \textit{Eq. 36}$$

$$\text{for each } P_{std}\,,$$

or finding $g(\lambda, i)$ independently of bracketing pressures P_1 and P_2 so that

$$g(\lambda, i\,)\rho_{gc}^*(\lambda, i, P_{1-2}) = \rho_{path}(\lambda, i, P_{1-2}) + t_d(\lambda, i, P_{1-2}\,)\ \cdot \rho_w(\lambda, i). \qquad \textit{Eq. 37}$$

Because one wants $\rho_w^{IS}(\lambda, i) = \ (1 - \epsilon(\lambda, i)\,) \cdot \rho_w(\lambda, P_1) + \epsilon(\lambda, i)\ \cdot \rho_w(\lambda, P_2)$, injecting the formulations Eq. 32 and Eq. 33 in both P_1 and P_2 branches leads to solve

$$g(\lambda,i)=\frac{\rho_w^{is}(\lambda,i)+(1-\varepsilon(\lambda,i))\frac{\rho_{path}(\lambda,P_1)}{t_d(\lambda,P_1)}+(\varepsilon(\lambda,i))\frac{\rho_{path}(\lambda,P_2)}{t_d(\lambda,P_2)}}{(1-\varepsilon(\lambda,i))\frac{\rho_{gc}^{*}(\lambda,P_1)}{t_d(\lambda,P_1)}+(\varepsilon(\lambda,i))\frac{\rho_{gc}^{*}(\lambda,P_2)}{t_d(\lambda,P_2)}},$$ *Eq. 38*

The implementation of the second choice was decided as it is the simplest and the closest to the implementation done on MERIS. However, question remains on the proper computation and validation of vicarious gains dedicated to high altitude water bodies.

3.2.4 Data preparation for the vicarious calibration of the visible bands

The in-situ datasets for vicarious adjustment have been selected with respect to their representativeness of world ocean Case 1 waters. We have chosen the MOBY (Brown et al., 2007) and BOUSSOLE (Antoine et al., 2006, 2008) buoys because they provide the longest time series of quality checked data in such conditions. Matchups extractions were made from the MERMAID system.

A reason to consider two sites is to dispose of the maximum of reference optical measurements. In some case it still might not be sufficient, especially when the system vicarious calibration is done shortly after the commissioning phase. The limitation of satellite coverage leads to a reduced number of exploitable matchups, in this case climatology datasets from GlobColour are used. Climatology matchups are done on oligotrophic part of the ocean to assure the homogeneity with the in-situ Case 1 waters datasets. Both types of matchups are processed the same way, without distinction.

3.2.4.1 Data matching and screening

We gather all OLCI 19x19 pixels box overpassing each site coordinates over the complete reprocessing duration. We then employ a nested box approach, by searching among macropixels with the less possible cloud, ice haze, high glint, and medium glint, finally keeping the 5x5 central pixels.

3.2.4.2 Denormalization procedure for the in-situ water-leaving reflectance

All in situ water-leaving reflectances come into a fully-normalized format, which means that the original measurements have been normalized to a zenith-illuminating / nadir-viewing geometry. For the comparisons with OLCI a denormalization procedure is used to transform the reflectance to that which would be measured in the acquisition geometry (both illuminating and viewing) of OLCI. The denormalization (described in (MERIS ATBD 2.9, n.d.)) is pixel-based and uses the same algorithm as the normalization of OLCI water-leaving reflectances.

3.2.5 Vicarious gains computation

Formulations Eq. 36 and *Eq. 38* are applied on the datasets mentioned above on an individual basis. Per match-up the uncertainty is given using the combination of the in situ and OLCI uncertainties:

$$u^2(g) = u^2(IS) + u^2(OCLI). \qquad \textit{Eq. 39}$$

In the lack of in situ measurements assessment of total uncertainty $u^2(IS)$is taken as 5% of $\boldsymbol{\rho_w^{is}(\lambda, i)}$. The OLCI uncertainty is taken as the dispersion within the collection of $\rho_w(\boldsymbol{\lambda}, \boldsymbol{i})$per match-up. Then the weight associated to an individual gain is

$$w(\lambda, i) = \frac{1}{u(g(\lambda,i))}, \qquad \textit{Eq. 40}$$

The higher the uncertainty, the lower the weight. The final gain is firstly computed per site using Eq. 24:

$$G(\lambda) = \frac{\sum_{i=1}^{N} w(\lambda,i) g(\lambda,i)}{\sum_{i=1}^{N} w(\lambda,i)}, \qquad \textit{Eq. 41}$$

with $g(\lambda, i))$ computed following the equation *Eq. 38*. We precise that we use the radiative transfer notations as expressed, as required, using AD-1. Such notations have already some mathematical simplifications of the radiative transfer that impacts the SVC gain uncertainty computation.

3.2.6 Gain uncertainty tree diagram

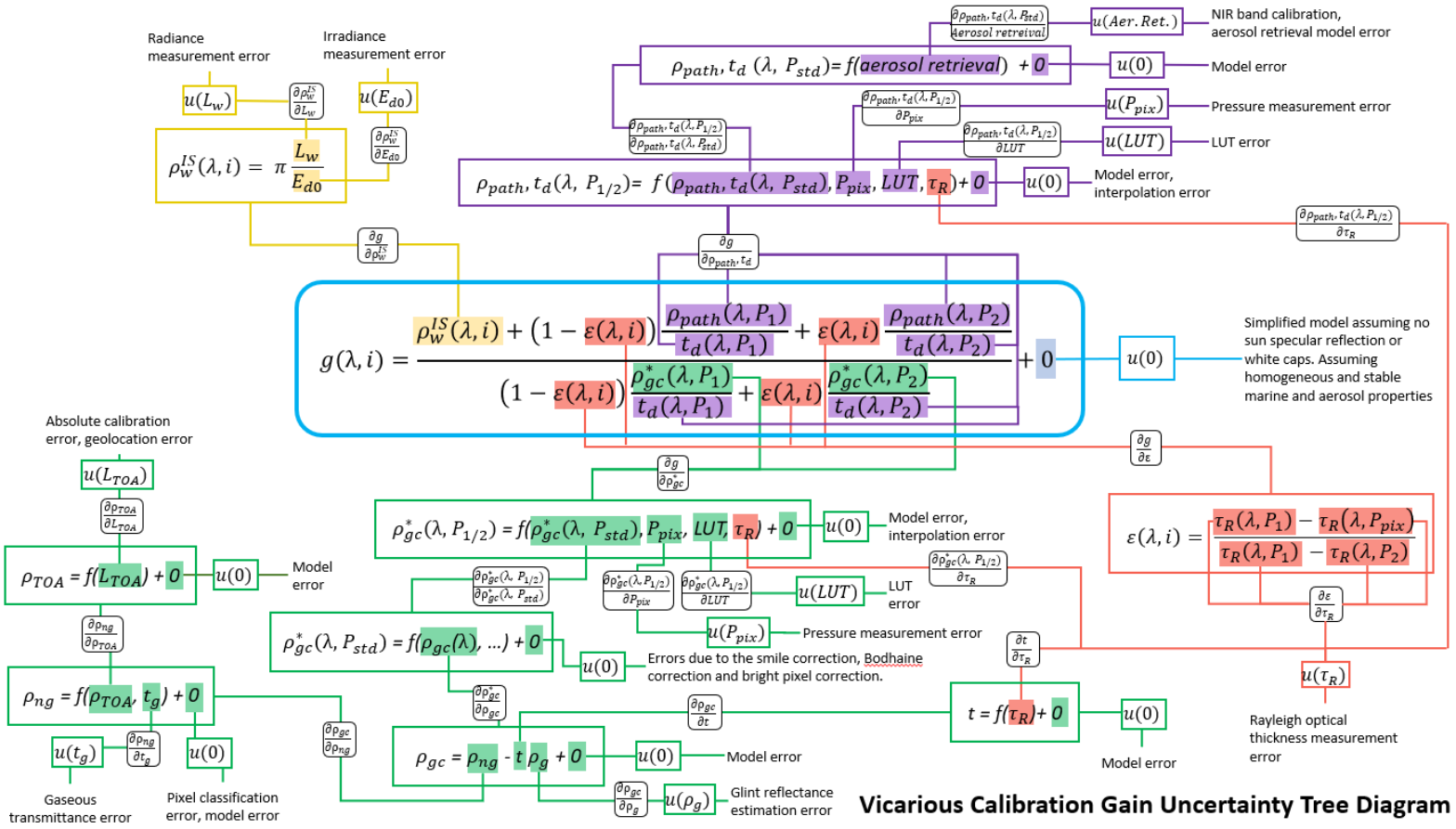

Figure 3-3. Vicarious Calibration Gain uncertainty tree diagram

4 Discussion of Uncertainty Contributions

In this section each source of uncertainty identified in the uncertainty tree diagram in Section 3.1.10 is analysed in turn using the "Effects Tables" structure described in Section 2.2. In cases where the full description of the analysis of an effect is beyond the scope of this document references are provided to an appropriate source or appendix. We use only one wavelength (490 nm) in the tables for brevity as the uncertainty magnitude value. Some uncertainties vary with wavelength thus for certain wavelength the values presented in the table might be too low.

Because of the complexity of the water leaving radiance processing many inputs are used in the measurement function multiple times. The sensitivity coefficients in the "Effects Tables" are defined as partial derivatives of a generic function, f. This function is not specified as depending on the step in the processing chain the function will change. The main goal of this EUB is to evaluate uncertainty in situ related to L_{w} thus the ultimate default function is water leaving radiance. However, it is important to note that uncertainty contributions will differently affect the various intermediate quantities calculated towards water leaving radiance, that are often also of interest. Table 4-1 presents an example with sensitivity coefficient for absolute radiometric calibration. This shows how the uncertainty related to the absolute radiometric calibration must be multiplied by a different sensitivity coefficient if one wants to evaluate uncertainty in K_{Lu} to the one that is used for L_{w}.

Table 4-1 – Example of changing sensitivity coefficients depending on the output of interest

Function/processing step	Sensitivity coefficients	
Generic one	$\frac{\partial f}{\partial c_{\mathrm{cal1}}}$	
Upwelling radiance	$\frac{\partial L_{\mathrm{u},z_1}}{\partial c_{\mathrm{cal1}}}$	$\frac{\partial L_{u,z_1}}{\partial c_{\mathrm{cal1}}} = \frac{1}{c_{cal1}} L_{\mathrm{u},z1}$
Attenuation coefficient	$\frac{\partial K_{\mathrm{Lu}}}{\partial c_{\mathrm{cal1}}}$	$\frac{\partial K_{\mathrm{Lu}}}{\partial c_{\mathrm{cal1}}} = \frac{1}{c_{\mathrm{cal1}}(z_2 - z_1)}$
Upwelling radiance just beneath the surface	$\frac{\partial L_{\mathrm{u}(0^-)}}{\partial c_{\mathrm{cal1}}}$	$\frac{\partial L_{u(0^-)}}{\partial c_{\mathrm{cal1}}} = \frac{1}{c_{cal1}} L_{u,z1} f_h \left(\frac{L_{\mathrm{u,z2}}}{L_{\mathrm{u,z1}}}\right)^{-z_1/(z_2-z_1)} \frac{z_2}{z_2 - z_1}$
Water leaving radiance	$\frac{\partial L_{\mathrm{w}}}{\partial c_{\mathrm{cal1}}}$	$\frac{\partial L_w}{\partial c_{cal1}} = \left(\frac{1-\rho}{n^2}\right) \frac{\partial L_{u(0^-)}}{\partial c_{\mathrm{cal1}}}$

4.1 *In situ* products

4.1.1 Upwelling radiance

4.1.1.1 Signal

The detector noise and dark current contribute to uncertainty in the raw digital numbers. In addition, when the instrument is operational *in-situ* the statistics of one-minute acquisition provide information about wave focusing and the instrument movement with the waves.

The *Table 4-2* presents an example of fully independent (uncorrelated) errors.

Table 4-2 – Effects table for detector noise

Table descriptor			
Name of effect		Noise in light counts	Night in dark counts
Affected term in measurement function		DN_{Light}	DN_{Dark}
Instruments in the series affected		All	All
Correlation type and form	Temporal within deployment	Random	Random
	Temporal between deployments	Random	Random
	Spectral (hyperspectral in-situ)	Random	Random
Correlation scale	Temporal within deployment	0	0
	Temporal between deployments	0	0
	Spectral (hyperspectral in-situ)	0	0
Channels/bands	List of channels / bands affected	All	All
	Error correlation coefficient matrix	Identity – No correlation	Identity – No correlation
Uncertainty	PDF shape	Gaussian	Gaussian
	units	Counts	Counts
	magnitude	Less than 0.1%	Less than 0.1%
Sensitivity coefficient		$\frac{\partial f}{\partial DN_{\mathrm{Light1}}}, \frac{\partial f}{\partial DN_{\mathrm{Light2}}}$	$\frac{\partial f}{\partial DN_{\mathrm{Dark1}}}, \frac{\partial f}{\partial DN_{\mathrm{Dark2}}}$

4.1.1.2 Instrument Calibration and Stability

Absolute radiometric calibration uncertainty is derived from the calibration measurements and the knowledge of the absolute standards. The level of calibration uncertainty is primarily defined by the quality of the standards used. Commonly used secondary standards such as FEL lamps and reflectance panels can provide absolute calibration uncertainty as the level of 2.5 % (k=2), this value can be reduced using a higher

quality standards as primary lamps calibrated directly by the NMI, or using a dedicated calibration integrating sphere with a transfer radiometer as proposed in ROSACE project for both types of calibration systems STAR-OCGE-CC and SMATR-CC. We anticipate achieving a level of 1.5% (*k*=2) for wavelengths above 420 nm. The absolute radiometric uncertainty is combined form systematic and random effects, we will spit then, so then the systematic part of that uncertainty will stay fully correlated between deployments (i.e. across calibrations) and the random part is correlated only within a deployment (i.e. between calibrations).

The stability of calibration is an additional component of uncertainty, that contains the information about temporal performance of the instrument i.e. if calibration holds during the deployment timeframe, how much the instrument responsivity changed. This can be only estimated during post deployment calibration and the records will build for each instrument over the time with their usage *in situ*. The evaluation of this effect is quite challenging, as needs to detect for a change that are smaller than the uncertainty of the calibration. Nominally, the calibration stability would be evaluated during a default calibration measurement, just the processing to retrieve this value is different.

The magnitude of calibration stability for each instrument is given by

$$\mathbf{c_{stab}} = \frac{\boldsymbol{c}_{\mathbf{cal},\mathbf{z}_1,t}}{\boldsymbol{c}_{\mathbf{cal},\mathbf{z}_1}} - \mathbf{1}, \qquad \textit{Eq. 42}$$

Where c_{cal,z_1} and $c_{\mathrm{cal},z_1,t}$ are pre and post deployment calibration coefficients.

To detect a change of the instrument radiometric responsivity at the level of 0.5% it is crucial to use the same stable source for both calibrations. The source needs to be monitored to ensure that the detected change can be attributed to the instrument and not to the source itself. The detailed information about the uncertainty of the radiance source is required to include the information about the systematic and random contributors.

The actual calibration stability will be modelled based on two calibration points defining its magnitude and series of *in situ* validation measurements that will define the shape of that function in time.

Table 4-3 – Effects table for detector calibration

Table descriptor				
Name of effect		Detector calibration systematic error	Detector calibration random error 1, 2	Detector calibration stability model error 1, 2
Affected term in measurement function		c_{cal,z_1}, c_{cal,z_2}, $c_{\mathrm{cal},z_1,t}$, $c_{\mathrm{cal},z_2,t}$	c_{cal,z_1}, c_{cal,z_2}, $c_{\mathrm{cal},z_1,t}$, $c_{\mathrm{cal},z_2,t}$	c_{stab,z_1}, c_{stab,z_2}
Instruments in the series affected		All	All	All
Correlation type and form	Temporal within deployment	Rectangular Absolute	Rectangular Absolute	Rectangular Absolute
	Temporal between deployments	Rectangular Absolute	Random	Random
	Spectral (hyperspectral in-situ)	To be defined	To be defined	To be defined
Correlation scale	Temporal within deployment	-∞,+∞	-∞,+∞	-∞,+∞
	Temporal between deployments	a,b[2]	0	0
	Spectral (hyperspectral in-situ)	To be defined	To be defined	To be defined
Channels/bands	List of channels / bands affected	All	All	All
	Error correlation coefficient matrix	Identity – No correlation	Identity – No correlation	Identity – No correlation
Uncertainty	PDF shape	Gaussian	Gaussian	Gaussian
	units	Radiance/Counts	Radiance/Counts	Radiance/Counts
	magnitude	0.70%	0.25%	Less than 1%
Sensitivity coefficient		$\frac{\partial f}{\partial c_{\mathrm{cal\_s}}}$	$\frac{\partial f}{\partial c_{\mathrm{cal\_r1}}}, \frac{\partial f}{\partial c_{\mathrm{cal\_r2}}}$	$\frac{\partial L_{\mathrm{w}}}{\partial c_{\mathrm{stab1}}}, \frac{\partial L_{\mathrm{w}}}{\partial c_{\mathrm{stab2}}},$

4.1.1.3 Instrument Characterisation

Additional instrument characterisation tests are planned for the initial pre-deployment phase and will be conducted at NPL using START-OCGE-CC facility with one exception of the immersion factor, that will be performed separately. The tests will check instruments performance and determine if any additional correction is needed. For example, if the detector linearity test result shows the detector linearity within the 0.1 % requirement than the additional correction is not needed. In the case when the detector linearity is 1% a correction coefficient will have to be applied to reduce this effect to required 0.1% level. Table 4-4 lists the characterisation errors that are assumed to be within the required specification range, then the

[2] When items a and b depend on recalibration schedule of the SMART -CC system

c $v$alues can have value of 1 and the uncertainty at the level of the test result. They all form systematic components of uncertainty.

Table 4-4 – Effects tables for detector characterisation

Table descriptor							
Name of effect		Spectral Calibration Error	Temperature Correction Error	Linearity Correction Error	Straylight Correction Error	Polarisation Correction Error	Immersion factor error
Affected term in measurement function		c_λ	c_T	c_lin	c_stray	c_pol	c_im
Instruments in the series affected		All	All	All	All	All	All
Correlation type and form	Temporal within deployment	Rectangular Absolute	Rectangular Absolute	Rectangular Absolute	Rectangular Absolute	Rectangular Absolute	Rectangular Absolute
	Temporal between deployments	Rectangular Absolute	Rectangular Absolute	Rectangular Absolute	Rectangular Absolute	Rectangular Absolute	Rectangular Absolute
	Spectral (hyperspectral in-situ)	To be defined	To be defined	To be defined	To be defined	To be defined	To be defined
Correlation scale	Temporal within deployment	-∞,+∞	-∞,+∞	-∞,+∞	-∞,+∞	-∞,+∞	-∞,+∞
	Temporal between deployments	-∞,+∞	-∞,+∞	-∞,+∞	-∞,+∞	-∞,+∞	-∞,+∞
	Spectral (hyperspectral in-situ)	To be defined	To be defined	To be defined	To be defined	To be defined	To be defined
Channels/bands	List of channels / bands affected	All	All	All	All	All	All
	Error correlation coefficient matrix	To be defined	To be defined	To be defined	To be defined	To be defined	To be defined
Uncertainty	PDF shape	Rectangular	Rectangular	Rectangular	Rectangular	Rectangular	Rectangular
	units	nm	%/degree	%	%	%	%
	magnitude	0.1 nm	negligible	0.2%	0.1%	negligible	negligible
Sensitivity coefficient		$\frac{\partial f}{\partial c_{\lambda 1}}, \frac{\partial f}{\partial c_{\lambda 2}}$	$\frac{\partial f}{\partial c_{\mathrm{T}1}}, \frac{\partial f}{\partial c_{\mathrm{T}2}},$	$\frac{\partial f}{\partial c_{\mathrm{lin}1}}, \frac{\partial f}{\partial c_{\mathrm{lin}2}}$	$\frac{\partial f}{\partial c_{\mathrm{stray}1}}, \frac{\partial f}{\partial c_{\mathrm{stray}}},$	$\frac{\partial f}{\partial c_{\mathrm{pol}1}}, \frac{\partial f}{\partial c_{\mathrm{pol}2}}$	$\frac{\partial f}{\partial c_{\mathrm{im}1}}, \frac{\partial f}{\partial c_{\mathrm{im}2}}$

4.1.2 Depth Measurement

Depth of the instruments on the buoy changes with the environmental conditions and it is evaluated per each measurement. The pressure, tilt and heading sensors errors can be spited into systematic that will come with the sensor calibration certificate, and random that are calculated form the statistics of measurements.

Table 4-5 – Effects tables for depth measurement error from sensors

Table descriptor									
Name of effect		Pressure sensor random error	Pressure sensor systematic error	Buoy tilt x random error	Buoy tilt x systematic error	Buoy tilt y random error	Buoy tilt x systematic error	Buoy heading random error	Buoy heading systematic error
Affected term in measurement function		z_{sensor}	z_{sensor}	θ_{x}	θ_{x}	θ_{y}	θ_{y}	ϕ	ϕ
Instruments in the series affected		All	All	All	All	All	All	All	All
Correlation type and form	Temporal within deployment	Random	Rectangular Absolute	Random	Rectangular Absolute	Random	Rectangular Absolute	Random	Rectangular Absolute
	Temporal between deployments	Random	Random	Random	Random	Random	Random	Random	Random
	Spectral	N/A	N/A	N/A	N/A	N/A	N/A	N/A	N/A
Correlation scale	Temporal within deployment	0	-∞,+∞	0	-∞,+∞	0	-∞,+∞	0	-∞,+∞
	Temporal between deployments	0	0	0	0	0	0	0	0
	Spectral (hyperspectral in-situ)	N/A	N/A	N/A	N/A	N/A	N/A	N/A	N/A
Channels/bands	List of channels / bands affected	All	All	All	All	All	All	All	All
	Error correlation coefficient matrix	To be defined	To be defined	To be defined	To be defined	To be defined	To be defined	To be defined	To be defined
Uncertainty	PDF shape	Gaussian	Gaussian	Gaussian	Gaussian	Gaussian	Gaussian	Gaussian	Gaussian
	units	%	%	degrees	degrees	degrees	degrees	degrees	0.5°

	magnitude	0.05%	0.1%	Various[3]	0.5°	Various	0.5°	Various	0.5°
Sensitivity coefficient		$\frac{\partial f}{\partial z_{\mathrm{sensor}}}$	$\frac{\partial f}{\partial z_{\mathrm{sensor}}}$	$\frac{\partial f}{\partial \theta_{\mathrm{x}}}$	$\frac{\partial f}{\partial \theta_{\mathrm{x}}}$	$\frac{\partial f}{\partial \theta_{\mathrm{y}}}$	$\frac{\partial f}{\partial \theta_{\mathrm{y}}}$	$\frac{\partial f}{\partial \phi}$	$\frac{\partial f}{\partial \phi}$

Instruments are manually mounted on the buoy structure for each deployment, at this stage distance measurements are taken errors related to this measurement for one deployment are always the same, thus this are systematic components, however they will become random between the deployments as a new set of distance measurement will be performed.

[3] Derived from the statistics of measurement, the value depends on environmental conditions and will vary.

Table 4-6– Effects tables for depth measurement error from pre-deployment measurements

Table descriptor						
Name of effect		Distance measurement error	Lower arm length error	Upper arm length error	Distance between arms error	Buoy heading offset
Affected term in measurement function		Δ_{SR}	Δ_2	Δ_1	Δ_{12}	ϕ_o
Instruments in the series affected		All	All	All	All	All
Correlation type and form	Temporal within deployment	Rectangular Absolute	Rectangular Absolute	Rectangular Absolute	Rectangular Absolute	Rectangular Absolute
	Temporal between deployments	Random	Random	Random	Random	Random
	Spectral	N/A	N/A	N/A	N/A	N/A
Correlation scale	Temporal within deployment	-∞,+∞	-∞,+∞	-∞,+∞	-∞,+∞	-∞,+∞
	Temporal between deployments	0	0	0	0	0
	Spectral (hyperspectral in-situ)	0	0	0	0	0
Channels/bands	List of channels / bands affected	All	All	All	All	All
	Error correlation coefficient matrix	Matrix of 1's – fully correlated	Matrix of 1's – fully correlated	Matrix of 1's – fully correlated	Matrix of 1's – fully correlated	Matrix of 1's – fully correlated
Uncertainty	PDF shape	Rectangular	Rectangular	Rectangular	Rectangular	Rectangular
	units	m	m	m	m	degrees
	magnitude	0.005 m	0.005 m	0.005 m	0.005 m	0.5 °
Sensitivity coefficient		$\frac{\partial f}{\partial \Delta_{SR}}$	$\frac{\partial f}{\partial \Delta_2}$	$\frac{\partial f}{\partial \Delta_1}$	$\frac{\partial f}{\partial \Delta_{12}}$	$\frac{\partial f}{\partial \phi_o}$

4.1.3 Models errors

Models used in the processing can have two types of errors, first related to the model's assumption and its correctness, these are presented in the Table 4-7. The second type is related to the uncertainty of the inputs to the models and these errors are listed in the Table 4-8.

Table 4-7– Effects tables for models' errors

Table descriptor						
Name of effect		Shading correction model error	Bio fouling correction model error	Hydrolight correction model error	Refractive index of seawater model error	Fresnel reflection model error
Affected term in measurement function		c_{sh}	c_{fou}	f_{h}	n	ρ
Instruments in the series affected		All	All	All	All	All
Correlation type and form	Temporal within deployment	Random	Rectangular Absolute	Random	Rectangular Absolute	Rectangular Absolute
	Temporal between deployments	Random	Random	Random	Rectangular Absolute	Rectangular Absolute
	Spectral (hyperspectral in-situ)	To be defined	To be defined	To be defined	To be defined	To be defined
Correlation scale	Temporal within deployment	0	a,b[4]	0	-∞,+∞	-∞,+∞
	Temporal between deployments	0	0	0	-∞,+∞	-∞,+∞
	Spectral (hyperspectral in-situ)	To be defined	To be defined	To be defined	To be defined	To be defined
Channels/bands	List of channels / bands affected	All	All	All	All	All
	Error correlation coefficient matrix	Identity – No correlation	Identity – No correlation	Identity – No correlation	Matrix of 1's – fully correlated	Matrix of 1's – fully correlated
Uncertainty	PDF shape	Gaussian	Gaussian	Gaussian	Gaussian	Gaussian
	units	%	%	%	%	%
	magnitude	2	negligible	0.5%	0.9[5]%	0.04% negligible
Sensitivity coefficient		$\frac{\partial f}{\partial c_{sh}}$	$\frac{\partial f}{\partial c_{\mathrm{fou}}}$	$\frac{\partial f}{\partial f_h}$	$\frac{\partial f}{\partial n}$	$\frac{\partial f}{\partial \rho}$

4.1.4 Inputs to various models used in the processing chain

The processing chain contains few models that are used to derive various corrections, like shading correction model, "Hydrolight" model, or estimation of the sea-air constant is derived from the modelled values of Fresnel reflectance and seawater refractive index. Each of this model depends on a few inputs and often one input quantity is used in several models (for example Chlorophyll concentration see Tree

[4] When items a and b depend on instrument cleaning schedule *in situ*

[5] When refractive index is considered wavelength independent

diagrams in section 3.1.10 for graphical representation). Thus, the water leaving radiance will depend on the errors in that input quantity that was used to modelled out correction.

Table 4-8 Effects tables for models' inputs errors

Table descriptor								
Name of effect		Chlorophyll concentration error	Solar Zenith Angle error	Seawater salinity	Atmospheric pressure error	Water Temperature error	Wind speed error	Viewing angle error
Affected term in measurement function		Chl	θ_{SZA}	salinity	P	T	w_{s}	θ_{V}
Instruments in the series affected		All	All	All	All	All	All	All
Correlation type and form	Temporal within deployment	To be defined	Rectangular Absolute	Rectangular Absolute	Rectangular Absolute	Rectangular Absolute	To be defined	To be defined
	Temporal between deployments	To be defined	Rectangular Absolute	Random	To be defined	To be defined	To be defined	To be defined
	Spectral (hyperspectral in-situ)	To be defined	To be defined	To be defined	To be defined	To be defined	To be defined	To be defined
Correlation scale	Temporal within deployment	-∞,+∞	-∞,+∞	-∞,+∞	-∞,+∞	-∞,+∞	-∞,+∞	-∞,+∞
	Temporal between deployments	-∞,+∞	-∞,+∞	0	0	-∞,+∞	-∞,+∞	-∞,+∞
	Spectral (hyperspectral in-situ)	To be defined	To be defined	To be defined	To be defined	To be defined	To be defined	To be defined
Channels/bands	List of channels / bands affected	All	All	All	All	All	All	All
	Error correlation coefficient matrix	Identity – No correlation	Identity – No correlation	Identity – No correlation	Identity – No correlation	Identity – No correlation	Identity – No correlation	Identity – No correlation
Uncertainty	PDF shape	Gaussian	Gaussian	Gaussian	Gaussian	Gaussian	Gaussian	Gaussian
	units	%	degrees	‰	mbar	°C	ms^{-1}	degrees
	magnitude	20	Negligible	Negligible	Negligible	Various	Various	Various
Sensitivity coefficient		$\frac{\partial f}{\partial Chl}$	$\frac{\partial f}{\partial SZA}$	$\frac{\partial f}{\partial salinity}$	$\frac{\partial f}{\partial P}$	$\frac{\partial f}{\partial T}$	$\frac{\partial f}{\partial W}$	$\frac{\partial f}{\partial \theta}$

4.1.5 Other quantities

The same methodology should be applied to all other quantities used in the processing chain. As presented in the sections above the water leaving radiance uncertainty contributors and their characteristics the same set of tables can be prepared for irradiance processing chain including all elements listed on the downwelling irradiance tree diagrams and for the gain calculation. This is beyond the scope of this document to list all the tables here, as the main idea here is to explain the methodology used in uncertainty budget evaluation.

5 Propagation of Uncertainties

There are two methods to propagate measurement uncertainty. One following the Law of Propagation of uncertainty (JCGM100:2008, 2008) sometimes called analytical approach, and the Monte Carlo Method (JCGM101:2008, 2008b). In fact, both of these methods are described in the GUM, with the difference that the original one uses analytical method to evaluate uncertainty and MCM method used numerical approach.

To evaluate the measurement uncertainty, regardless of the chosen method, several steps need to be taken:

1. A measurement function must be defined,
2. All sources of uncertainty must be identified.
3. Then according to the Law of Propagation of Uncertainty (see Eq. 2) sensitivity coefficients must be calculated. Nominally, sensitivity coefficient is a partial derivative of a measurement function and a given contributor. For complex function it might be impossible to calculate these coefficients analytically. This step is not needed for Monte Carlo approach.
4. Using the analytical method all inputs uncertainty with PDF different than normal shape must be converted to that shape. To do that a divisor is specified for usual shapes for example to convert a rectangular PDF to its equivalent in Normal distribution an uncertainty value is divided by $\sqrt{3}$. This step is not needed when Monte Carlo method is used, and the original PDF can be propagated thought the model.
5. If there any of the inputs' quantities are correlated with each other, then an error covariance matrix is necessary (see Eq. 4).
6. To combine uncertainties Eq. 2 is used for the analytical approach. In MCM approach the measurements function is run many times, each time uses the randomly selected inputs form previously defined PDFs of the input quantities.
7. The results of the analytical approach by default have a Gaussian distribution and when quoted as the output of Eq. 2 is called standard uncertainty, that means this has a coverage factor k=1, or 1σ defined as one standard deviation from the mean assuming a normal distribution function. This information expresses the confidence level at 67% that the estimated value is within its quoted uncertainty. The result in the MCM is a PDF of the output quantity, depending of its shape the uncertainty is defined as standard deviation of this distribution (Gaussian PDF) or by the upper and lower limits that define 67% coverage of that distribution.

8. For some application higher confidence is necessary, then the standard uncertainty is expanded to *k*=2 for 95% coverage or *k*=3 to 99% coverage. This than called expanded uncertainty

Practical implementation of these steps can vary depending on application. To propagate uncertainty for the measurands of interest of this project (L_w, L_{wN}, g, and mission averaged gain) we propose the following approach

1. Measurement functions are defined based on the tree diagrams including all raw inputs (see section 3.1.10). Where the raw inputs are defined as quantities that can have an influence on the measurand values. These are used for all processing steps rather that intermediate quantities (for example K_{Lu} in calculation of L_w).
2. All raw inputs have their standard uncertainty identified in terms of magnitude (value) and PDF shape
3. Due to complexity of the measurement function it is challenging to derive all sensitivity coefficients analytically (for example $\frac{\partial L_w}{\partial Chl}$ or $\frac{\partial L_w}{\partial z_{sensor}}$ would be extremely difficult), thus we propose to use MCM to propagate the raw inputs uncertainties using a measurement function. However, to meet the project requirement and provide the EUB calculation in Microsoft Excel document we use the measurement function defined for the MCM to evaluate sensitivity coefficients on each input value. This approach is known as finite-difference formulae (SWSPEC- MS-7 appendix B), where the sensitivity coefficient can be approximated using the following formula:

$$\left.\frac{\partial \boldsymbol{f}}{\partial \boldsymbol{X_i}}\right|_{\boldsymbol{X=x}} \approx \frac{\boldsymbol{f_i}(\boldsymbol{x_i}+\boldsymbol{\delta_i})-\boldsymbol{f_i}(\boldsymbol{x_i}-\boldsymbol{\delta_i})}{\boldsymbol{2\delta_i}}, \qquad \textit{Eq. 43}$$

here $\delta_i = u(x_i)$

4. To complete the EUB.xslx calculation spreadsheet the divisors are provided for the input components uncertainties.
5. We handle the partial correlation between some input quantities (for example, the absolute radiometric calibration coefficients of the different instruments) by decomposing these to a set of variables that are independent of each other (though these independent variables may themselves be correlated through time). The details of this for each input quantity are described in the previous section.
6. The final uncertainty value will be derived from PDF of MCM as well as the simple sum of squares of all independent inputs, averaged accordingly to their temporal correlation scale (i.e. some of the input will be correlated within one deployment, whereas others might be correlated all the time)

7. Results will be presented for each observation including detailed information about the random, systematic within deployment and systematic components. The uncertainty for time averaged products will be reported with at the same level of details.
8. All uncertainties will be reported with the k=1 coverage factor.

5.1 Intended Excel document (EUB.xlsx) user guide

The Excel document was intended to be prepared to accompany this document and to provide all calculations used for the evaluation of EUB. A draft EUB.xlsx was presented on the midterm review on this project and the remaining text in this section outlines the concept proposed back then to translate the methodology of measurements uncertainty evaluation proposed in preceding sections of this document. The complexity of the processing chain and the flexibility of proposed MCM that automatically derives sensitivity coefficients for all input components, dynamically changes the values of uncertainty sources related to change of the input component magnitude and deal with error correlation made the Excel version of the EUB always lacking some information and proving that translation extremely difficult.

The Excel document was aligned with the measurement equations presented here. The worksheet "Itemzied components" contains a list of effects that have been identified in this document, the same symbolic notation is used. Following the methodology presented here, information about each uncertainty component contains is sensitivity coefficient, information about its PDF shape that automatically link to the divider value. Then each of the listed items is assigned to one of the components class. The classes are defined now as random, fully correlated within one deployment and fully correlated in mission lifetime.

The uncertainties will be evaluated for L_{w}, E_s and ρ_w as an output of the field segment, ρ_{wN} as the input to the gain calculation, individual match up gain and mission average gain. They will be reported as one value for each of that four outputs, and then they spitted into the 3 categories described above. For example, for L_{w} uncertainty will be presented as

$$\mathbf{u}^2(\boldsymbol{L}_{\mathbf{w}}) = \mathbf{u}^2_{\mathbf{random}}(\boldsymbol{L}_{\mathbf{w}}) + \mathbf{u}^2_{\mathbf{d\ sys}}(\boldsymbol{L}_{\mathbf{w}}) + \boldsymbol{u}^2_{\mathbf{sys}}(\boldsymbol{L}_{\mathbf{w}}) \,, \qquad \textit{Eq. 44}$$

Where each category has several inputs

$$\boldsymbol{u}^2_{\mathbf{random}}(\boldsymbol{L}_{\boldsymbol{w}}) = \boldsymbol{c}_1^2\left(\frac{\mathbf{u}(\boldsymbol{x}_1)}{\boldsymbol{d}_1}\right)^2 + \boldsymbol{c}_2^2\left(\frac{\mathbf{u}(\boldsymbol{x}_2)}{\boldsymbol{d}_2}\right)^2 + \ldots + \boldsymbol{c}_n^2\left(\frac{\mathbf{u}(\boldsymbol{x}_n)}{\boldsymbol{d}_n}\right)^2 \,, \qquad \textit{Eq. 45}$$

Where c represents sensitivity coefficients (column F in EUB.xlsx) x in uncertainty value of a given components (columns L-X, as these varies spectrally in EUB.xlsx) and d is the divisor (column H in EUB.xlsx).

The time averaged product for example mission averaged gain will be calculated including different temporal correlation terms.

$$\boldsymbol{u^2(\bar{g}) = \frac{\sum_i u^2_{\mathrm{rand}}(g_i)}{N} + \frac{\sum_j \left[\frac{1}{N_j}\sum_k u_{\mathrm{d\,sys}}(g_k)\right]^2}{M} + \left[\frac{1}{N}\sum_i u_{\mathrm{sys}}(g_i)\right]^2} \quad , \qquad \textit{Eq. 46}$$

Where $\bar{g}$ is the mission average gain, g_i is individual match up gain, N is the total number of match ups and $M$is a number of deployments that have correlated inputs. N_j is the number of match-ups in a given deployment, j, where g_k are the subset of individual match ups in that deployment.

Please note that this equation might be split up into further components to account for odd and even deployments, since measurements may be correlated in a differently depending if they are in an odd and even deployment. In addition, the match up gain from second site can be added here, then g in equation **Eq. 46** will be replaced by g_1 and g_2 to represent site 1 and site 2, each of them will have individually calculated random and systematic components.

6 Results

6.1 In situ products

The demonstration data set used to obtain these results is from BOUSSOLE *in situ* hyperspectral data that were classified for the SVC process for Sentinel 3A covering the period from May 2016 until March 2017. During that time 20 valid match ups were find.

Figure 6-1 presents the range of the sun illumination and the S3A viewing geometries.

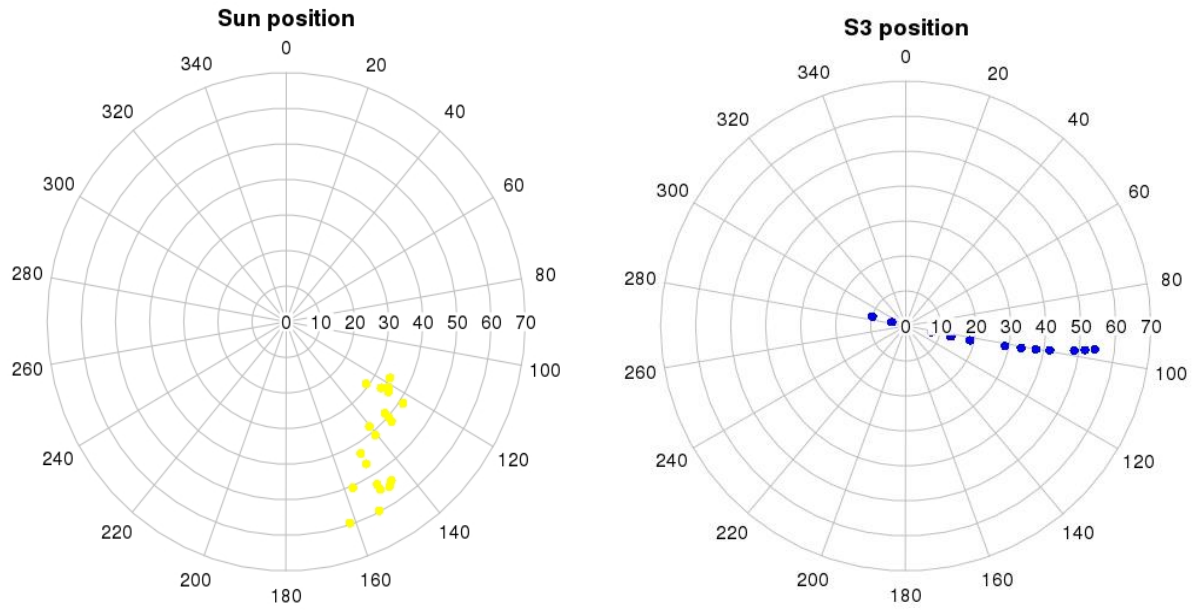

Figure 6-1. Left- the sun illumination geometries for the data in the study dataset, right S3 viewing geometries for the data in the study dataset.

6.1.1 Water leaving radiance

The uncertainties presented here are obtained using MCM described in section 5 Propagation of Uncertainties and applying the scheme presented in the water leaving reflectance tree diagram presented in Figure 3-1.

The water leaving radiance uncertainties for each measurement point in the study data for the first 9 spectral bands on S3 are presented in Figure 6-2.

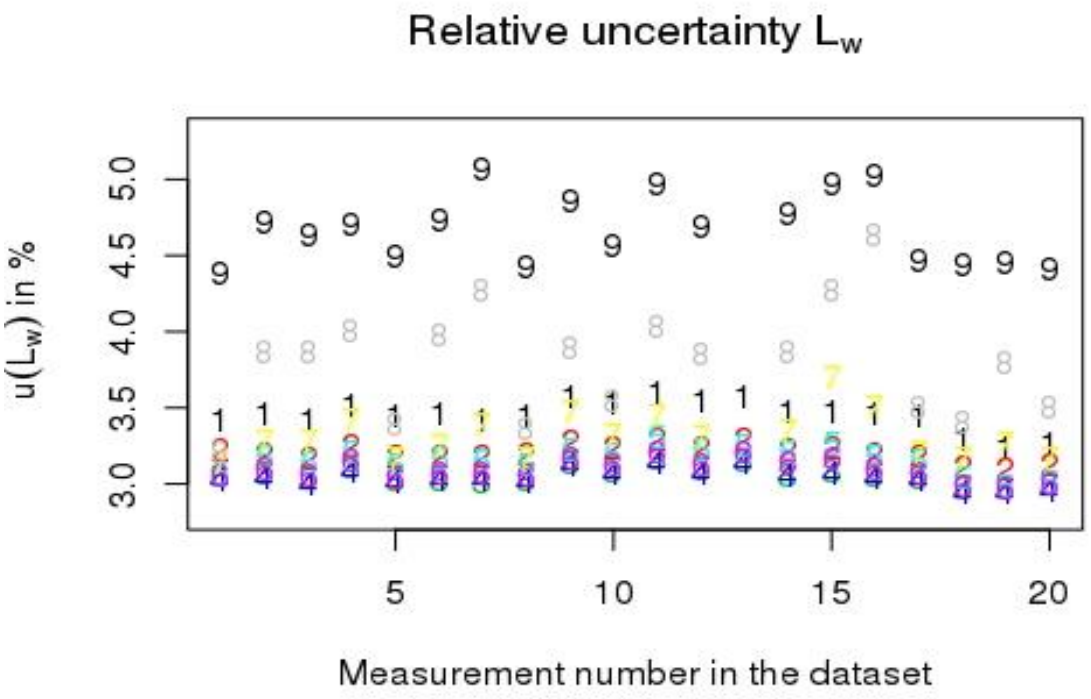

Figure 6-2. Relative uncertainties (k=1) for the water leaving radiance per measurements. The numbers indicate spectral bands where 1 is 400 nm band and 9 is 681 nm band.

These uncertainties are evaluated using existing absolute calibration capabilities, which would be could be significantly improved.

6.1.2 Downwelling irradiance

The uncertainties presented here are obtain using MCM described in steps in section 5 Propagation of Uncertainties and applying the scheme presented in the downwelling irradiance tree diagram presented in Figure 3-2.Figure 2-1

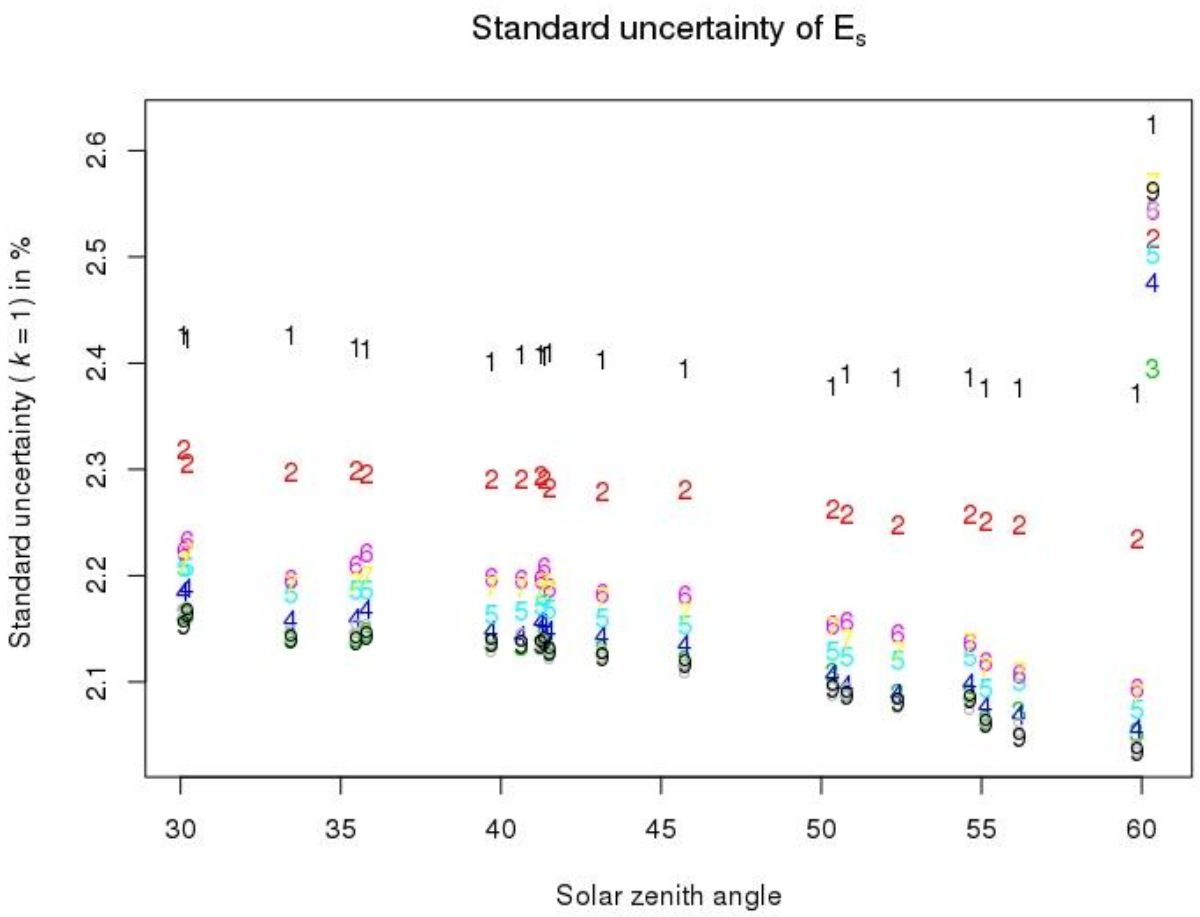

Figure 6-3. Relative uncertainties (k=1) for the water leaving radiance plotted against SZA. The data series numbers indicate spectral bands where 1 is 400 nm band and 9 is 681 nm band.

The value of uncertainty in downwelling irradiance is sensitive to the SZA. Which is an effect of the changes to the ratio of the direct to total downwelling radiation and sensitivity of the buoy tilt correction to SZA.

The spectral channels 1 - 400 nm and 2 – 412 nm, where the diffuse component is the highest are less sensitive to SZA. One measurement point has significantly higher uncertainty, which is the effect of SZA during in situ measurement being 60,3° and the uncertainty in cosine response of the diffuser in the current scheme have higher values assign for the SZA above 60.

6.1.3 Water leaving reflectance

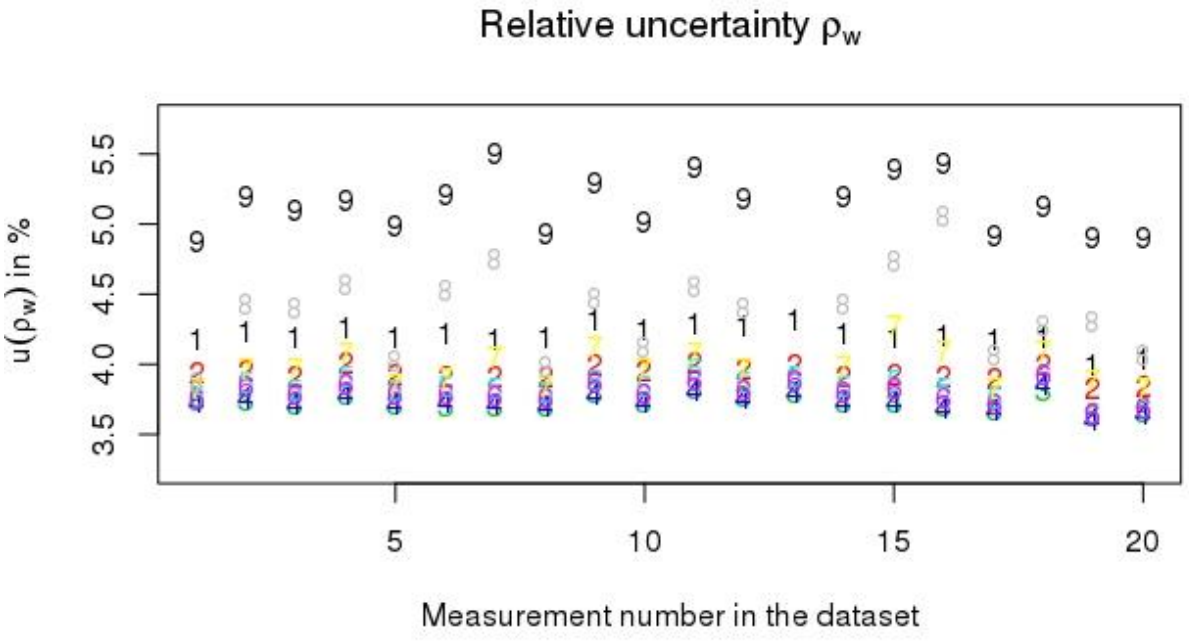

Figure 6-4. Relative uncertainties (k=1) for the water leaving reflectance plotted against measurements number in the dataset. The data series numbers indicate spectral bands where 1 is 400 nm band and 9 is 681 nm band.

6.2 Gain estimates

6.2.1 Initial approach

The basis for EUB calculation were defined in [AD-1] Requirements for Copernicus Ocean Colour Vicarious Calibration Infrastructure (Mazeran, Brockmann, Ruddick, Voss, & Zagolski, 2017a) document, where the main *in situ* variable is fully normalised water leaving radiance, L_{wN}. The gain calculation as well as the individual gain uncertainy calculation is then based on , L_{wN}, according to the equation below:

$$u(g) = \frac{t_g t\, \mu_s C_s C_Q^t L_{wN}^t}{L_t} \sqrt{\left(\frac{u(L_{wN}^t)}{L_{wN}^t}\right)^2 + \left(\frac{u(C_Q^t)}{C_Q^t}\right)^2}$$

eq 26 in AD-1

6.2.2 Actual OLCI Processing

One of the outcomes from mid-term review was the clear request from the reviewers to include downwelling irradiance, E_s, and remote sensing reflectance, R_{rs}, in the EUB in addition to fully normalised water leaving radiance, L_{wN}, as clearly these are needed for the gain calulation. We did not dissuss the detail of the gain calculation method at that time, but the need for E_s and R_{rs} can clearly be seen in the OLCI SVC processing, where the gain is calculated as:

$$g(\lambda, i) = \frac{\rho_{gc}^t(\lambda,i)}{\rho_{gc}(\lambda,i)}, \qquad \textit{Eq. 47}$$

Not, as in eq.13 from AD-1

$$g(\lambda, i) = \frac{L_t^t(\lambda,i)}{L_t(\lambda,i)}, \qquad \textit{Eq. 48}$$

The individual gain uncertainty in OLCI processing is then calculated as described in section 3.2.5 Vicarious gains computation.

Issues with current Uncertainty Calculations

Neither of the above methods for calculating uncertainty is fully correct in terms of GUM methodology:

- Eq 26 from AD-1 correctly estimates the uncertainy in individual gain due to in situ contribution and BRDF correction only, assuming that there is no other sources of uncertainy related to the atmospheric or TOA signal. Most critically however, this equation is only valid for the gain processing defined in AD-1, which uses water leaving radiance, not reflectance.

- Eq. 16 from the actual OLCI processing contains *in situ* and TOA in reflectance, but as a simple sum of squares. This does not take into account the real measurement equation used to derive the gain and omits the atmosphere as well.

Note – the assumption of equivalence of the gaseous transmittance and, L_{path}, lays at the heart of the current SVC methodology and therefore by default the atmospheric contribution to gain uncertainty is typically not addressed (though in the proposal for this work we did aim to look into this atmospheric contribution).

Way Forward

Therefore, since the existing [AD-1] uncertainty equation is not applicable to the OLCI SVC processing from ACRI, and the current ACRI uncertainty model does not follow the GUM methodology. NPL proposed to use the schematic presented in Figure 3-3. Vicarious Calibration Gain uncertainty tree diagram, that uses the actual measurement equation for the individual gain for OLCI. This solution was started to be evaluated in R software and proved to be challenging to be delivered on time with sufficient confidence in the results to be presented. NPL will continue to work on this solution beyond the completion of the project and report the results when they become internally validated.

7 Conclusions

This document described the approach to calculate uncertainty budget for *in situ* measurement of water leaving radiance performed in water at fixed depths and accompanied with downwelling irradiance measurements to enable *in situ* remote sensing reflectance derivation in the need for the vicarious calibration gain. The GUM methodology (JCGM100:2008, 2008; JCGM101:2008, 2008a) and its newest application presented in FIDUCEO project (Mittaz et al., 2019) for the climate data records were proposed as a robust solution for a complex Ocean Colour Radiometry measurement process. MCM was chosen to perform the calculations, enabling addressing often omitted error correlation contribution to the overall uncertainty value.

The proposed methodology addresses in details uncertainty propagation process, considering the temporal scale correlations present in mission averaged gain calculation. The practical realisation of that method can be introduced in the data processing chain and would enable uncertainty per measurements evaluation, always including appropriate ancillary data. This method provides a concept of dynamic uncertainty per in situ measurement and match – up.

The ambitious methodology proved to be challenging in few aspects. Firstly, to be fully investigated and applied for the gain calculation in a limited timeframe of this project. Secondly to be literally impossible to convert to excel calculation spreadsheet.

The results were presented on a small subset of the current BOUSSOLE in situ measurements and its current capabilities. It is envisaged that the upgrade of the instrumentation and calibration/characterisation proposed within the ROSACE project will reduce the presented numbers further. The radiometric calibration uncertainty is one of the major contributors to the overall value.

The proposed option of two sites will allow to double the number of match ups per year. Both sites equipped with the same instrumentation will have capability of equally good quality measurements with the similar uncertainties. Due to the difference in their environmental condition the numbers of the lowest uncertainty measurements can slightly vary.

8 Bibliography

Antoine, D., Chami, M., Claustre, H., D'Ortenzio, F., Morel, A., Bécu, G., … and Darrell Adams. (2006). *BOUSSOL}: A Joint CNRS-INSU, ESA, CNES, and NASA Ocean Color Calibration and Validation Activity*. Goddard Space Flight Center Greenbelt, Maryland 20771: NASA.

Antoine, D., Guevel, P., Deste, J.-F., Becu, G., Louis, F., Scott, A. J., & Bardey, P. (2008). The "BOUSSOLE" buoy - A new transparent-to-swell taut mooring dedicated to marine optics: Design, tests, and performance at sea. *JOURNAL OF ATMOSPHERIC AND OCEANIC TECHNOLOGY*, *25*(6), 968–989. https://doi.org/10.1175/2007JTECHO563.1

Antoine, D., & Morel, A. (1999). A multiple scattering algorithm for atmospheric correction of remotely sensed ocean colour (MERIS instrument): Principle and implementation for atmospheres carrying various aerosols including absorbing ones. *International Journal of Remote Sensing*, *20*(9), 1875–1916. https://doi.org/10.1080/014311699212533

Austin, R. W. (1974). The remote sensing of spectral radiance from below the ocean surface. In N. G. Jerlov & E. Steemann-Nielsen (Eds.), *Optical Aspects of Oceanography* (pp. 317– 344). Elsevier, New York.

Bailey, S. W., Hooker, B. H., Antoine, D., Franz, B. A., & Werdell, P. J. (2008). Sources and assumption for the vicarious calibration of ocean color satellite observations. *Applied Optics*, *Vol. 47,*(No. 12), 2035 – 2045.

Brown, S. W., Flora, S. J., Feinholz, M. E., Yarbrough, M. A., Houlihan, T., Peters, D., … Clark, D. K. (2007). The marine optical buoy ({MOBY}) radiometric calibration and uncertainty budget for ocean color satellite sensor vicarious calibration. *Proc.SPIE*, *6744*, 6744-6744–12. https://doi.org/10.1117/12.737400

Clark, D. K., Gordon, H. R., Voss, K. J., Ge, Y., Broenkow, W., & Trees, C. (1997). Validation of atmospheric correction over the oceans. *Journal of Geophysical Research: Atmospheres*, *102*(D14), 17209–17217. https://doi.org/10.1029/96JD03345

Cox, C., & Munk, W. (1954). Statistics of the sea surface derived from Sun glitter,. *Journal of Marine Research, 13*, 198 – 227.

Franz, B. A., Ainsworth, E. J., & Bailey, S. W. (2001). *SeaWiFS, vicarious calibration: an alternative approach utilizing simultaneous in situ observations of oceanic and atmospheric optical, properties*. National Aeronautics, and Space Administration, Goddard Space Flight Center, Greenbelt, MD.

Franz, B. A., Bailey, S. W., Werdell, P. J., & McClain, C. R. (2007). Sensor-independent approach to the vicarious calibration of satellite ocean color radiometry. *Appl. Opt.*, *46*(22), 5068–5082.

https://doi.org/10.1364/AO.46.005068

Gordon, H. R. (1997). Atmospheric correction of ocean color imagery in the Earth Observing System era. *Journal of Geophysical Research: Atmospheres*, *102*(D14), 17081–17106. https://doi.org/10.1029/96JD02443

Gordon, H. R. (1998). In-Orbit Calibration Strategy for Ocean Color Sensors. *Remote Sensing of Environment*, *63*(3), 265–278. https://doi.org/https://doi.org/10.1016/S0034-4257(97)00163-6

Gordon, H. R., & Clark, D. K. (1981). Clear water radiances for atmospheric correction of coastal zone color scanner imagery. *Appl. Opt.*, *20*(24), 4175–4180. https://doi.org/10.1364/AO.20.004175

JCGM100:2008. (2008). *Evaluation of measurement data - Guide to the expression of uncertainty in measurement*.

JCGM101:2008. (2008a). *Evaluation of measurement data - Supplement 1 to the ``Guide to the expression of uncertainty in measurement'' - Propagation of distributions using a Monte Carlo method*.

JCGM101:2008. (2008b). *Evaluation of measurement data - Supplement 1 to the "Guide to the expression of uncertainty in measurement"' - Propagation of distributions using a Monte Carlo method."*

JCGM200:2012. (2012). *International vocabulary of metrology – Basic and general concepts and associated terms*.

Mazeran, C., Brockmann, C., Ruddick, K., Voss, K., & Zagolski, F. (2017a). *Requirements for {C}opernicus {O}cean {C}olour {V}icarious {C}alibration {I}nfrastructure*.

Mazeran, C., Brockmann, C., Ruddick, K., Voss, K., & Zagolski, F. (2017b). *Requirements for Copernicus Ocean Colour Vicarious Calibration Infrastructure*.

MERIS ATBD 2.13. (n.d.). *Sun Glint Flag Algorithm*.

MERIS ATBD 2.9. (n.d.). *Pigment index retrieval in case 1 waters.*

Mittaz, J., Merchant, C. J., & Woolliams, E. R. (2019). Applying principles of metrology to historical Earth observations from satellites. *Metrologia*, *56*(3), 032002. https://doi.org/10.1088/1681-7575/ab1705

Mittaz, J., Taylor, M., Desmons, M., & Woolliams, E. (2017). *FIDUCEO D2.2 (AVHRR): Report on the AVHRR FCDR uncertainty*.

Mobley, C. D. (1994). *Light and water: radiative transfer in natural waters*. Academic press.

Morel, A., & Gentili, B. (1996). Diffuse reflectance of oceanic waters. {III}. Implication of bidirectionality for the remote-sensing problem. *Appl. Opt.*, *35*(24), 4850–4862. https://doi.org/10.1364/AO.35.004850

Mueller, J. L., Fargion, G. S., McClain, C. R., Clark, D. K., Yuen, M., Kuwahara, V. S., … Barnes, R. A. (2003). *Ocean Optics Protocols For Satellite Ocean Color Sensor Validation, Revision 4, Volume V: Special Topics in Ocean Optics Protocols and Appendices*. Goddard Space Flight Center Greenbelt, Maryland 20771: NASA.

Santer, R., & Zagolski, F. (2017). *Technical note on pressure adjustment*.

Woolliams, E., Mittaz, J., Merchant, C., & Harris, P. (2018). *FIDUCEO D2.2a: Principles behind the FCDR effects table*.

Appendix A - FIDUCEO CORRELATION FORMS

Within any one of the dimensions described in Section 2.2.2, the error correlation can take different forms. Within the FIDUCEO project a set of error correlation forms, sufficiently close to those expected in reality, were defined to represent the expected error correlation in practical cases. The error correlation form describes the correlation coefficient between any two measured values in the dimension for which it is defined.

The defined error correlation forms are (taken from Woolliams et al. (2017)):

- **Random:** In this there is no error correlation with any other measured value.
- **Rectangular absolute (contains systematic):** In this the error correlation is constant for a particular range of values defined absolutely, rather than relative to the measured value. This includes the following cases:
    - Where a single measured value is used over an explicit range, e.g. where a single calibration value is used for all measurements over several scanlines, or in a particular year, and a different calibration value is used for all measurements outside that range.
    - For an effect that is fully systematic in that dimension (common to all measured values in that dimension). This is described with the dimensions $[-\infty,+\infty]$
- **Triangular relative:** In this the error correlation drops linearly (in the dimension of interest) relative to a particular measured value. This comes from a running average with constant weights.
- **Bell-shaped relative:** In this the error correlation drops faster than linearly (in the dimension of interest) relative to a particular measured value. This can come from:
    - A weighted running average (e.g. over neighbouring scanlines), which weights the central reading more than the others involved in the average.
    - Any other form of weighted averaging (e.g. through a spline fit in geolocation)
    - Other cases where our expectation is that the correlation drops off over distance in some way.

  In none of these cases is the error correlation form exactly Gaussian, but a truncated Gaussian form is a practical approximation for the Bell-shaped form, and is used. What this correlation form represents is the situation where “nearby” errors are relatively highly correlated, but this correlation drops off over a distance. By defining the Gaussian width and the truncation range (beyond which there is no error correlation), it is possible to define a reasonable range of realistic correlation forms.

- **Repeating rectangles:** This comes from something for which the error correlation coefficient is constant within a small range (1 pixel or a range of pixels), then repeats on a regular cycle. It could

come from a push-broom sensor where every *n*th scanlines are from a common detector element, or from a seasonal affect that occurs annually.

- **Repeating bell-shapes:** This is another repeating effect, but one where locally there is a drop off of correlation (partially correlated with neighbouring pixels/scanlines) which then has a repeating effect.
- **Stepped triangle absolute:** This accounts for the situation, for example in the FIDCUEO HIRS (High-resolution Infrared Radiation Sounder) FCDR, where there is a calibration cycle, so that the instrument measures the calibration target once every certain number of scanlines, and then there is a rolling average between scanlines. The correlation to neighbouring scanlines takes the form of a stepped triangle.
- **Other:** Although true correlation structures may be more complicated than the ones given above, the above are sufficiently representative for the correlation structures encountered in FIDUCEO thus far. However, there may be situations where an FCDR producer needs to define a new error correlation form.

Depending on the type of error correlation form, different information is required. This is listed in Table A-1, below.

Table A-1 – Parameters defined for different correlation forms

Correlation form	Parameters	Description
random	none required	For fully random effects there is no correlation with any other pixel
rectangle_absolute	**[-a,+b]** (rectangle limits). Provide these per pixel/scanline/orbit as required. Allow for a way of representing **[-∞,+∞]** **[rmax]** States correlation coefficient for all pixel / scanline / orbit pixels. Default is rmax = 1 (fully correlated)	An effect is systematic within a range and different outside that range. For each pixel / scanline / orbit in range say number of pixels / etc either side that it shares a correlation with. For fully systematic effects notation to say "systematic with all". If rmax is defined, then the correlation coefficient is one for the pixel with itself, and is rmax with all other pixels.
triangle_relative	**[n]** – number of pixels/scanlines being averaged in simple rolling average (should be an odd number)	Suitable for rolling averages over a window from (–n-1)/2 to (+n-1)/2 (i.e. for n pixels/scanlines being averaged) Assumes a simple mean, not a weighted mean.

		No rmax is needed, since it is always 1.
bell_shaped_relative	**[n]** – number of pixels being averaged in a weighted rolling average, from which truncation range and standard deviation for Gaussian representation follow (truncation beyond ±n pixels, $\sigma = \frac{n/2-1}{\sqrt{3}}$) (n should be odd) OR **[n,sigma]** n: truncation from –n to +n, sigma: width of Gaussian representation (n should be odd) Typically provided once per orbit file (some further consideration needed about first/last scanlines in an orbit)	Suitable for rolling averages over a window from (–n-1)/2 to (+n-1)/2 (i.e. for n pixels/scanlines being averaged). Assumes a weighted mean, for any weights (and thus also includes things like spline fitting). Also suitable for anything else where the assumption is that "closer pixels/scanlines are more correlated than further pixels". This can use two terms – n gives the truncation range outside which the assumption is there is no (or negligible) correlation, and sigma gives how fast the correlation drops off.
repeating_rectangles	**[-a,+b,rmax,L,h,imax]** per pixel/scanline/orbit etc (rmax,L,h will be same for different pixels)	Correlation coefficient assumed to be rmax for pixels/scanlines from –a to +b, and h for pixels/scanlines from L-a to L+b and from 2L-a to 2L+b and so on (iL-a to iL+b) for all integers i up to imax.
repeating_bell_shapes	**[n,sigma,L,h, imax]**	Correlation coefficient assumed to drop off as a truncated Gaussian for local pixels/scanlines etc in the range defined by n and a similar Gaussian with a peak of h and the same width for pixels/scanlines iL pixels apart on either side, for all integers I up to imax.

stepped_triangle_absolute	**[-a,+b,n]** per pixel/scanline/orbit etc (n will be same for different pixels)	The step is a rectangular absolute from –a to +b with a correlation coefficient of one, after which the correlation coefficients drops for another a+b+1 lines, and then again. n is the number of calibration windows averaged.
Other	A function describing the correlation	Not yet implemented.